HAL open science

Assessing practical identifiability during calibration and cross-validation of a structured model for high-solids anaerobic digestion

Vicente Pastor-Poquet, Stefano Papirio, Jérôme Harmand, Jean-Philippe Steyer, Eric Trably, Renaud Escudié, Giovanni Esposito

To cite this version:

Vicente Pastor-Poquet, Stefano Papirio, Jérôme Harmand, Jean-Philippe Steyer, Eric Trably, et al.. Assessing practical identifiability during calibration and cross-validation of a structured model for high-solids anaerobic digestion. Water Research, 2019, 164, 10.1016/j.watres.2019.114932 . hal-02623443

HAL Id: hal-02623443

https://hal.inrae.fr/hal-02623443

Submitted on 20 Dec 2021

HAL is a multi-disciplinary open access archive for the deposit and dissemination of scientific research documents, whether they are published or not. The documents may come from teaching and research institutions in France or abroad, or from public or private research centers.

L'archive ouverte pluridisciplinaire **HAL**, est destinée au dépôt et à la diffusion de documents scientifiques de niveau recherche, publiés ou non, émanant des établissements d'enseignement et de recherche français ou étrangers, des laboratoires publics ou privés.

Distributed under a Creative Commons Attribution - NonCommercial 4.0 International License

Version of Record: https://www.sciencedirect.com/science/article/pii/S0043135419307067
Manuscript_701a48311e91fad1d86a1eeeb213be9f

Assessing Practical Identifiability during Calibration and Cross-Validation of a Structured Model for High-Solids Anaerobic Digestion

Vicente Pastor-Poquet [a,b,*], Stefano Papirio [c], Jérôme Harmand [b], Jean-Philippe Steyer [b], Eric Trably [b], Renaud Escudié [b], and Giovanni Esposito [c]

[a] Department of Civil and Mechanical Engineering, University of Cassino and Southern Lazio, via Di Biasio 43, 03043 Cassino (FR), Italy

* Corresponding author. E-mail: vicente.pastor.poquet@gmail.com

[b] LBE, Univ. Montpellier, INRA, 102 Avenue des Etangs, 11100, Narbonne, France

[c] Department of Civil, Architectural and Environmental Engineering, University of Napoli Federico II, via Claudio 21, 80125 Napoli, Italy

ABSTRACT

High-solids anaerobic digestion (HS-AD) of the organic fraction of municipal solid waste (OFMSW) is operated at a total solid (TS) content ≥ 10 % to enhance the waste treatment economy, though it might be associated to free ammonia (NH_3) inhibition. This study aimed to calibrate and cross-validate a HS-AD model for homogenized reactors in order to assess the effects of high NH_3 levels in HS-AD of OFMSW, but also to evaluate the suitability of the reversible non-competitive inhibition function to reproduce the effect of NH_3 on the main acetogenic and methanogenic populations. The practical identifiability of structural/biochemical parameters (i.e. 35) and initial conditions (i.e. 32) was evaluated using batch experiments at different TS and/or

© 2019 published by Elsevier. This manuscript is made available under the CC BY NC user license
https://creativecommons.org/licenses/by-nc/4.0/

inoculum-to-substrate ratios. Variance-based global sensitivity analysis and approximate Bayesian computation were used for parameter optimization. The experimental data in this study permitted to estimate up to 8 biochemical parameters, whereas the rest of parameters and biomass contents were poorly identifiable. The study also showed the relatively high levels of NH_3 (i.e. up to 2.3 g N/L) and ionic strength (i.e. up to 0.9 M) when increasing TS in HS-AD of OFMSW. However, the NH_3 non-competitive function was unable to capture the acetogenic/methanogenic inhibition. Therefore, the calibration emphasized the need for target-oriented experimental data to enhance the practical identifiability and the predictive capabilities of structured HS-AD models, but also the need for further testing the NH_3 inhibition function used in these simulations.

Keywords: High-solids Anaerobic Digestion Model; Ammonia Inhibition; Ionic Strength; Global Sensitivity Analysis; Approximate Bayesian Computation.

1 INTRODUCTION

High-solids anaerobic digestion (HS-AD) of the organic fraction of municipal solid waste (OFMSW) is operated at total solids (TS) ≥ 10 % to minimize the reactor volume, the water addition and the digestate dewatering (Pastor-Poquet et al., 2019a). HS-AD can also lead up to 80 % TS removal, easing the digestate post-treatment. However, HS-AD of OFMSW is usually associated to free ammonia (NH_3) inhibition, resulting in volatile fatty acids (VFA) accumulation. NH_3 affects both acetoclastic and hydrogenotrophic methanogens but also the rest of VFA degraders (acetogens) in anaerobic digestion (AD), being the inhibition related to the operative parameters (i.e. temperature and pH) and the biomass acclimation (Rajagopal et al., 2013).

Adding lignocellulosic materials to OFMSW permits to minimize the buildup of total ammonia nitrogen (TAN), while their low hydrolysis rates permit to increase the TS content and to counteract the VFA accumulation in HS-AD (Capson-Tojo et al., 2017; Pastor-Poquet et al., 2019a). However, including lignocellulosic waste in OFMSW depends on the season or the local waste management strategy. Whether or not a lignocellulosic co-substrate is used, understanding the effects of NH_3 inhibition is crucial to optimize HS-AD of OFMSW.

A HS-AD model was recently developed for homogenized reactors to evaluate the NH_3 inhibition in HS-AD of OFMSW (Pastor-Poquet et al., 2018, 2019b). This structured model, based on the Anaerobic Digestion Model No. 1 (ADM1) (Batstone et al., 2002), gathers the main bio-physical-chemical mechanisms in HS-AD. In the HS-AD model, apparent (i.e. kmol/kg H_2O) instead of global (i.e. kmol/kg) concentrations determine

the effect of TS upon solutes, as a consequence of the low water content within HS-AD. Meanwhile, an extended set of mass balances allows the simulation of the organic mass removal from the biogas production. A liquid solution 'non-ideality' subroutine was subsequently included in the model as a function of the ionic strength (*I*), since 'non-ideality' determines the pH, CO_2 liquid-gas transfer and NH_3 inhibition in HS-AD (Pastor-Poquet et al., 2019b). As a preliminary assumption, the HS-AD model included a reversible non-competitive inhibition function by NH_3 (I_{nh3}) [Equation 1] in the biochemical rates of acetogenic and methanogenic populations, a mathematical resource commonly used in structured AD models (Astals et al., 2018).

$$I_{nh3} = \frac{K_{i,Snh3}}{K_{i,Snh3} + S_{nh3,App}} \quad (1)$$

Simulating the NH_3 inhibition at high TS with the HS-AD model requires an adequate set of input parameters, θ, to be estimated by calibration (Pastor-Poquet et al., 2018, 2019b). θ includes both the structural/biochemical parameters, θ_P, and the initial and influent conditions, θ_B: $\theta = (\theta_P, \theta_B)$. Nonetheless, calibration of structured AD models is not trivial due to the equation complexity and large number of θ involved (Dochain & Vanrolleghem, 2001; Donoso-Bravo et al., 2011).

To calibrate a mathematical model, θ must be structurally and practically identifiable, instead of correlated. The θ structural identifiability is theoretically assessed, assuming noise-free experimental data and error-free model structure. Noteworthy, nearly all θ in ADM1 are (locally) structurally identifiable (Nimmegeers et al., 2017). This is a prerequisite to assess the θ practical identifiability and calibrate the HS-AD model using

'imperfect' experimental data. Unfortunately, the reduced number of experimental data often available and/or the presence of experimental errors yield non-identifiable parameters; i.e. parameters that cannot be uniquely estimated. These are known as practical identifiability issues.

Calibration usually consists of minimizing an objective function, $J(\theta)$, that condenses the 'goodness of fitting' between the experimental data, y, and the model outputs, $y^{sim}(\theta)$, being these a function of N input parameters, θ (Dochain & Vanrolleghem, 2001; Flotats et al., 2010). Several $J(\theta)$ can be used to calibrate AD models as the weighted sum of squares or any user-defined alternative (Donoso-Bravo et al., 2011; Ratto et al., 2001). Assuming the existence of a global minimum (optimum) for an objective function, $J(\theta_{opt})$, this value is reached using the optimal set of input parameters, θ_{opt}.

Practical identifiability issues commonly translate into $J(\theta)$ showing many local optimums and/or flat valleys, where the precise value of θ cannot be easily determined (Guisasola et al., 2006; Rodriguez-Fernandez et al., 2006). Thus, only practical identification of a reduced θ subset (i.e. $N' < N$) is often possible for ADM1-based models (Nimmegeers et al., 2017). This is called model over-parameterization, where the modification of two individual θ, θ_i (with $i = 1, \ldots, N$), can lead to a similar model output. Particularly, when using batch experiments – highly dependent on the initial conditions – to calibrate AD models, different sets of experimental conditions, including different inoculum-to-substrate ratios (ISR), are required to reduce the θ correlation (Donoso-Bravo et al., 2011; Flotats et al., 2010).

Two main approaches can be used to calibrate complex models: the Bayesian and the frequentist. The frequentist approach searches for optimal θ values, θ_{opt}, whereas the Bayesian approach considers θ_{opt} as probabilistic distributions conditioned on the experimental data, $p(\theta_{opt}|y)$, instead of single values (Ratto et al., 2001; Rodriguez-Fernandez et al., 2006; Saltelli et al., 2006). In both approaches, when facing over-parameterization, it must be assessed which θ_i significantly influence $y^{sim}(\theta)$ (sensitivity analysis) and need to be adequately calibrated.

ADM1-based models contain several θ_P (i.e. ≥ 35) and θ_B (i.e. ≥ 24). θ_P might be obtained from literature, though a different model structure – from where these θ_P were obtained – potentially influences the optimal θ_P values/distributions (Pastor-Poquet et al., 2019b). On the other hand, θ_B might not be easily determined due to the lack of experimental data or the difficulties to translate the data into adequate model units (Donoso-Bravo et al., 2011; Flotats et al., 2003).

Parameter inference based on the Bayes' theorem [Equation 2] is particularly suited to calibrate structured AD models since it can deal with complex $J(\theta)$ showing several optima or flat geometries, where frequentist inference might not be well suited (Kennedy & O'Hagan, 2001; Toni & Stumpf, 2010). In Bayesian inference, the prior parameter distribution, $p(\theta)$, is sampled to obtain the posterior parameter distribution, $p(\theta|y)$, conditioned on the experimental data, y, and the likelihood function, $p(y|\theta)$, while $p(y)$ can be considered as a normalizing constant. Importantly, any user-defined $J(\theta)$ arising from $p(y|\theta)$ can be used in 'informal' statistical approaches [Equation 3], as

variance-based global sensitivity analysis (GSA) and approximate Bayesian computation (ABC) (Donoso-Bravo et al., 2011; Nott et al., 2012).

$$p(\theta|y) = \frac{p(y|\theta)p(\theta)}{p(y)} \quad (2)$$

$$J(\theta) = f(p(y|\theta)) \quad (3)$$

Variance-based GSA provides an appropriate assessment about the potentiality of θ_i to influence the model outputs and the correlations existing with the rest of θ, θ_j (with j = 1, …, N and $i \neq j$) (Kennedy & Petropoulos, 2017; Oakley & O'Hagan, 2004). Similarly, ABC permits also to highlight practical identifiability issues yielding simultaneously the most likely $p(\theta|y)$ (Beaumont et al., 2009; Filippi et al., 2013; Toni & Stumpf, 2010). As main disadvantage, Bayesian inference is often computationally intensive.

The mathematical performance of the HS-AD model was previously verified, though the model was only validated for a single HS-AD batch experiment due to the elevated number of θ requiring calibration (i.e. > 30) (Pastor-Poquet et al., 2018, 2019b). Instead, this study aimed to fully calibrate and cross-validate the HS-AD model to simulate the effect of high NH_3 levels in HS-AD of OFMSW, while testing the non-competitive NH_3 inhibition function [Equation 1] on the main acetogenic/methanogenic populations. In particular, this study assessed the practical identifiability of 35 θ_P and 32 θ_B, by using nine HS-AD batch digesters at different TS and/or ISR as a source of experimental data. Identifiability was assessed by variance-based GSA and ABC permitting to approximate also $p(\theta|y)$. Importantly, the proposed methodology can be easily readapted to account for further HS-AD datasets (e.g. batch, continuous) and/or model configurations.

156

157 **2 METHODOLOGY**

158 **2.1 Experimental Data**

159 To calibrate and cross-validate the HS-AD model, while further evaluating the effects of
160 increasing the initial TS content on HS-AD simulations, four different batch
161 experiments were used at thermophilic (55ºC) conditions from 10 to 30 % TS [Table 1].
162 The laboratory-scale reactor design volume ($V_{Reactor}$) was either 160 or 280 mL for the
163 different experiments. In all experiments, centrifuged inoculum was used to increase
164 simultaneously the initial TS and ISR. These small-scale digesters were manually
165 shaken when the biogas production was measured. The batch experiments are described
166 next, whereas a thorough description of these experiments and the bio-physical-
167 chemical analyses performed was reported elsewhere (Pastor-Poquet et al., 2019a).

168

169 Experiment 1 consisted of a sacrifice test for mono-digestion of OFMSW using ISR =
170 1.00 g VS/g VS. In this experiment, the main physical-chemical dynamics (i.e. biogas
171 production and composition, TS, VS, VFA, TAN, and mono-valent ions) were
172 evaluated at different operational times. In Experiments 2 to 4, the biogas production
173 and composition were measured at different experimental times, whereas the rest of
174 physical-chemical analyses (i.e. TS, VS, VFA, TAN and ions) were only performed
175 before starting and after ending each experiment. Non-sacrifice experiments included
176 mono-digestion of OFMSW using ISR = 1.50 g VS/g VS (Experiment 2) and ISR =
177 0.50 g VS/g VS (Experiment 3), but also co-digestion of OFMSW and beech sawdust
178 using ISR = 0.16 g VS/g VS (Experiment 4).

179

180 Within Experiments 2 and 4, different initial TS contents – dilutions – were evaluated,
181 though all the initial batch conditions contained exactly the same amount of substrate
182 and centrifuged inoculum. Briefly: 1) the inoculum was centrifuged; 2) the same
183 amount of substrate and inoculum was added to each bottle; 3) distilled water was
184 added to reach the different TS contents; and 4) each bottle was manually homogenized.
185 This strategy was aimed to use the mass balances among the different initial TS
186 conditions, as explained in Section 2.3.1, since soluble materials were partially removed
187 when centrifuging the inoculum. In total, nine different HS-AD batch conditions were
188 assessed at different TS, ISR and/or co-digestion ratios, subsequently named as "Batch
189 No. 1 to 9" [Table 1].
190

191 **2.2 HS-AD Model**

192 The HS-AD model included the main biochemical rates of Pastor-Poquet et al. (2018),
193 though some minor modifications were also implemented [Table 2]. Firstly, a reversible
194 non-competitive NH_3 inhibition function [Equation 1] was included in the valeric (S_{va}),
195 butyric (S_{bu}), propionic (S_{pro}), and hydrogen (S_{h2}) uptake rates, similarly to the NH_3
196 (S_{nh3}) inhibition on the acetate (S_{ac}) uptake, aiming to simulate the VFA accumulation
197 observed in HS-AD experiments likely consequence of the NH_3 buildup (Pastor-Poquet
198 et al., 2019a). Secondly, carbohydrates (X_{ch}) were split into readily-biodegradable
199 ($X_{ch,fast}$) and slowly-biodegradable ($X_{ch,slow}$) to simulate the relatively lower hydrolysis
200 rates of sawdust and the longer methane production observed in co-digestion
201 experiments (i.e. ≥ 200 d) [Table 1]. Importantly, the hydrolysis of both $X_{ch,fast}$ and
202 $X_{ch,slow}$ pooled into soluble sugars (S_{su}).
203

204 **2.3 Model Calibration and Validation**

205 A common set of biochemical parameters was used for all HS-AD simulations at
206 different ISR and/or TS. All biochemical parameters for thermophilic (55ºC) AD were
207 extracted from Batstone et al. (2002), though some of those needed to be calibrated (i.e.
208 θ_P) to improve the model fitting. The initial conditions of the batch experiments were
209 predefined according to the experimental data available, as described by Pastor-Poquet
210 et al. (2018) and also mentioned next. Moreover, different ranges of initial biomass
211 concentrations were used (i.e. θ_B) to assess the potential interrelationship of θ_B with θ_P
212 in batch experiments.

213

214 **2.3.1 Initial Conditions**

215 The initial conditions used for each batch simulation are shown in Table 3. Since the
216 same amount of substrate and inoculum was used along different initial TS contents in
217 Experiment 2, but also in Experiment 4, mass balances were used to reduce the number
218 of 'unknown' initial conditions [Table 1]. To use mass balances, the anaerobic
219 biodegradability (BD) of each substrate-inoculum mixture in Experiment 2 and
220 Experiment 4 was assumed constant, whereas the soluble (S) and particulate (X)
221 components were assumed proportional, among the different TS contents. With these
222 assumptions, mass balances permitted to extrapolate the molar and chemical oxygen
223 demand (COD) concentrations as a function of the initial reactor content mass (M_{Global}),
224 reactor content specific weight (ρ_{Global}) and reactor content volume (V_{Global}). For
225 example, the concentration of acetoclastic methanogens (X_{ac}) in Batch No. 3 was
226 approximated from Batch No. 2 as: $X_{ac,Batch3} = X_{ac,Batch2} \cdot V_{Global,Batch2}/V_{Global,Batch3}$.

227

228 The nitrogen content of soluble (S_i) and particulate (X_i) inert in each substrate-inoculum
229 mixture ($N_{i,subs}$) determined the initial protein (X_{pr}) + amino-acid (S_{aa}) content,
230 according to the nitrogen balance, as shown elsewhere (Pastor-Poquet et al., 2018).
231 Thus, $N_{i,subs}$ was different for each batch experiment [Table 3]. On the other hand,
232 despite the initial conditions of batch experiments were maintained for all the
233 simulations, different biomass concentrations (i.e. degraders of sugars, X_{su}; amino acids,
234 X_{aa}; long-chain fatty acids, X_{fa}; valerate, X_{c5}; butyrate, X_{bu}; propionate, X_{pro}; acetate,
235 X_{ac}; and hydrogen, X_{h2}) were also assessed, as mentioned before. Since mass balances
236 were used among different TS in Experiments 2 and 4, only the initial conditions of
237 Batch No. 1, 2, 6 and 7 [Table 1] were evaluated.
238

239 **2.3.2 Biochemical Parameters, Biomass Concentrations and Calibration Ranges**

240 The modified biochemical parameters (θ_P) and modified biomass concentrations (θ_B) in
241 this study, including their initial values and potential variability ranges, are shown in
242 Table 4. In total, 35 θ_P and 32 θ_B were evaluated. θ_P related to the hydrolysis, sugar
243 fractioning (f_{su}), maximum growth rate (k_m) and half-saturation constant (K_S), but also
244 the pH, NH_3 and H_2 inhibition constants (K_i), since all these θ_P are simultaneously
245 associated to the substrate under study, are correlated among themselves, and strongly
246 regulate the biogas production/composition from solid substrates (Batstone et al., 2002;
247 Garcia-Gen et al., 2015). On the other hand, θ_B included all the initial biomass
248 concentrations in the HS-AD simulations (i.e. X_{su}, X_{aa}, X_{fa}, X_{c5}, X_{bu}, X_{pro}, X_{ac} and X_{h2}),
249 as these concentrations might not only strongly influence the biogas production during
250 the initial days of batch experiments, but might also be potentially interrelated among
251 themselves and/or to the previous θ_P.

The sugars uptake yields butyrate ($f_{bu,su}$), propionate ($f_{pro,su}$), acetate ($f_{ac,su}$) and hydrogen ($f_{h2,su}$) as COD fractions in ADM1. Therefore, a maximum of three fractions can be selected simultaneously to fulfill the COD balance: $f_{bu,su} + f_{pro,su} + f_{ac,su} + f_{h2,su} = 1$. In this study, $f_{bu,su}$, $f_{ac,su}$ and $f_{h2,su}$ were selected, while $f_{pro,su}$ was recalculated: $f_{pro,su} = 1 - f_{bu,su} - f_{ac,su} - f_{h2,su}$. Importantly, further structural parameters and initial conditions need to be induced in the HS-AD model as, for example, the amino-acid (AA, S_{aa}) fractioning and the biomass yield coefficients (Y_b), though these were not assessed here aiming to reduce the problem under study. In either case, the proposed methodology for calibration/validation can easily include any further θ.

Variability ranges for structural parameters are suggested in ADM1 (Batstone et al., 2002). However, considerably wider ranges were assessed in this study to emphasize the absence of prior knowledge about the optimal values. For simplicity, all θ_P were allowed to vary by 90 % from their initial values, $\theta_{P,0}$: $(1 - 0.9) \cdot \theta_{P,0} \leq \theta_P \leq (1 + 0.9) \cdot \theta_{P,0}$; uniform $p(\theta_P)$ [Table 4]. As the only exception, the lower pH threshold for acetoclastic methanogens ($pH_{LL,ac}$) was bounded between a pH value where methanogenesis potentially collapses (i.e. ≤ 5.0) and the upper pH threshold for acetoclastic methanogens ($pH_{UL,ac}$, i.e. 7.0), to maintain the suitability of the Hill function to simulate the pH inhibition [Table 2].

Different methods are available to approximate the initial conditions (i.e. biomass concentrations) in batch simulations as, for example, simulating a continuous reactor fed with exactly the same substrate until reaching steady state, and then use these steady

conditions to initialize the batch simulations (Dochain & Vanrolleghem, 2001; Donoso-Bravo et al., 2011). However, since the inoculum was centrifuged right before setting the batch experiments in this study, absence of prior knowledge about the initial biomass concentrations was preferred. To explore homogeneously different orders of magnitude in the biomass concentrations (often $0 < \theta_B < 1$ kmol COD/m^3), the logarithm-transformed θ_B were allowed to vary by 50 % from their initial values, $\theta_{B,0}$: $(1 + 0.5) \cdot log_{10}(\theta_{B,0}) \leq log_{10}(\theta_B) \leq (1 - 0.5) \cdot log_{10}(\theta_{B,0})$; uniform $p(log_{10}(\theta_B))$ [Table 4].

2.3.3 Objective Function

The weighted sum of squares between all the available experimental and the corresponding simulated values was used as objective function, $J(\theta)$ [Equation 4]. $J(\theta)$ was adapted from Flotats et al. (2003) to assess the model 'goodness of fitting', being: θ the structural parameters and/or initial conditions implemented in the HS-AD model; R the number of batch simulations; D the number of experimental datasets; t_{exp} the experimental time of each batch experiment; $y_{i,j,t}$ the experimental measurements; $y_{i,j,t}^{sim}(\theta)$ the simulated values; and $w_{i,j}$ the weighting coefficients – calculated as a function of the average experimental data, $\bar{y}_{i,j}$ [Equation 5]. With this approach, $J(\theta)$ was lower-bounded by the – preliminarily unknown – global minimum: $J(\theta) \geq J(\theta_{opt})$.

$$J(\theta) = \sum_{i=1}^{R}\sum_{j=1}^{D}\sum_{t=t_1}^{t_{exp}} w_{i,j}\left(y_{i,j,t} - y_{i,j,t}^{sim}(\theta)\right)^2 \tag{4}$$

$$w_{i,j} = \frac{1}{\sum_{t=t_1}^{t_{exp}}\left(y_{i,j,t} - \bar{y}_{i,j}\right)^2} \tag{5}$$

Noteworthy, only 6 out of 9 experimental conditions were used to calculate $J(\theta)$ in this study: Batch No. 1, 3, 5, 6, 7 and 9 [Table 1]. Meanwhile, 3 out of 9 experimental

conditions were used for cross-validation: Batch No. 2, 4 and 8 [Table 1]. Other experimental combinations could be used for calibration/cross-validation as, for example, Batch No. 2, 4, 5, 7 and 8 for calibration and Batch No. 1, 3, 6 and 9 for cross-validation. However, the configuration used in this study permitted to include the most extreme HS-AD conditions for model calibration (i.e. TS $\leq$ 10 %, TS $\geq$ 30 %), while intermediate conditions (i.e. 10 $\leq$ TS $\leq$ 30 %) were used for cross-validation. This strategy also aimed to enhance the number of experimental data used for calibration and to ensure the most diverse operative conditions where θ might be representative. Additionally, the proposed configuration included the most informative dataset (i.e. Batch No. 1) to increase the complexity of $J(\theta)$ and remove identifiability issues related to the lack of bio-physical-chemical dynamics in the overall dataset, as further discussed in Section 3.1.3.

2.3.4 Global Sensitivity Analysis

GSA was aimed to highlight the most influential θ to be calibrated with the available set of experimental data. For GSA, multiple θ combinations were used to evaluate $J(\theta)$ [Equation 4]. Latin-hypercube sampling (LHS) served to explore the global θ space (Solon et al., 2015). Subsequently, $J(\theta)$ arrays and their corresponding θ were assessed by the GSA engine of Kennedy and O'Hagan (2001) and Oakley and O'Hagan (2004). The GSA engine calculates the individual (IE) and global (GE) effects of θ_i upon the global model output (e.g. $p(y|\theta)$, $J(\theta)$) variance. On the other hand, the GSA engine provides also all the double correlations between θ_i and θ_j (i.e. $\theta_i \cdot \theta_j$, being $i \neq j$). Both IE and $\theta_i \cdot \theta_j$ are expressed as a percentage of the global variance explained. Thus, θ_i showing a relatively low IE are associated to poor practical identifiability, since these θ_i

influence minimally the model output. Meanwhile, GE comprises IE, the double correlations $\theta_i \cdot \theta_j$ and all the rest of multiple correlations for a single θ_i. Therefore, GE itself should not be used to assess the identifiability. Instead, the overall correlation of θ_i with θ can be inferred by the relative difference between IE and GE – though IE and GE are expressed in different units, as interactions can be repeated in the GE of two or more θ_i (Oakley & O'Hagan, 2004; Saltelli et al., 2006). Summarizing, both a low IE and a large IE to GE difference mean poor identifiability for a single θ_i, though *a priori* no fixed threshold – neither for IE, nor for GE minus IE – permits to distinguish whether θ_i should be considered as non-identifiable.

A maximum θ subset of $N' = 30$ and/or 400 simulations of $J(\theta)$ can be evaluated simultaneously with the GSA engine (Kennedy & Petropoulos, 2017). Therefore, to assess θ interactions when $N > 30$, a combination strategy was followed. Firstly, 30 θ_i were randomly selected and evaluated by GSA (i.e. GSA No. 1). From these θ, only those showing the smallest IE (e.g. < 1 %) were disregarded as non-identifiable, removed from the initial θ subset, and not used for further GSA. Importantly, these non-identifiable θ_i were fixed at their initial values [Table 4] for all subsequent model simulations, since non-identifiability implies that these θ can be fixed at any value within $p(\theta)$ (Dochain & Vanrolleghem, 2001; Guisasola et al., 2006). Then, θ_P and/or θ_B non-previously-assessed by GSA were combined with the non-removed θ subset, and a new GSA was performed (i.e. GSA No. 2). The GSA methodology was repeated until the last remaining θ subset was considered as 'potentially identifiable', θ'.

In total, seven GSA with different θ combinations were progressively performed [Table 5]. In this study, the only criterion for non-identifiability was assumed as IE ≤ 0.20 %, which also coincided with a relatively low GE (i.e. < 4.5), though this conservative criterion could be modified as mentioned in Section 3.1.1. To enhance the GSA representativeness in presence of a high number of θ (i.e. $20 \leq N' \leq 30$) and/or wide variability ranges (i.e. ± 50 %), each GSA was conducted in triplicate and the results averaged. Finally, all $J(\theta)$ arrays used for GSA were searched for the minimum observed value, $J_{min}(\theta)$ (i.e. $\geq J(\theta_{opt})$), to be subsequently used in ABC.

2.3.5 Approximate Bayesian Computation

The θ' posterior distribution, $p(\theta'|y)$, was assessed by ABC (Toni & Stumpf, 2010). In short, multiple simulations were carried at different θ' combinations sampled by LHS, whereas relatively high $J(\theta')$ values were discarded by a progressively stringent criterion based in a tolerance coefficient, ε (i.e. > 1.0). In other words, only $J(\theta') - J_{min}(\theta') \leq \varepsilon$ were accepted for posterior evaluation: $p(\theta'|J(\theta') - J_{min}(\theta') \leq \varepsilon)$. With this approach, θ' identifiability was further assessed by the convergence in the confidence range.

In this study, ε was successively reduced from 2.50 to 1.05 (i.e. 2.50, 1.80, 1.30, 1.10 and 1.05). Within each explored $J(\theta') - J_{min}(\theta') \leq \varepsilon$ range, 400 simulations were used. θ' were allowed to vary within the same range used for GSA [Table 4]. Meanwhile, the 5 to 95 % interquartile range of each θ' was used as confidence range, but also as a criterion for identifiability/convergence. The posterior mean, median, mode, Kurtosis,

Skewness and correlation matrix were also evaluated, as described in Martin and Ayesa (2010).

2.3.6 Cross-Validation

Cross-validation assesses the model 'goodness of fitting' in experiments not used for calibration (Bennett et al., 2013). In this study, the θ' posterior mean was considered as θ_{opt}. Thus, θ_{opt} were used to simulate all batch experiments, including the three experimental conditions selected for cross-validation: Batch No. 2, 4 and 8 [Table 1].

3 RESULTS AND DISCUSSION

3.1 GSA – Selecting the Most Influencing Input Parameters for Calibration

3.1.1 Preliminary Identifiability Assessment

GSA results are summarized in Table 5. GSA was started with 30 θ_P and progressively led to only 14 θ': 13 θ_P (i.e. $K_{h,pr}$, $K_{h,ch,slow}$, $k_{m,fa}$, $k_{m,c5}$, $k_{m,c4}$, $k_{m,pro}$, $k_{m,ac}$, $k_{m,h2}$, k_d, $pH_{LL,ac}$, $f_{bu,su}$, $f_{ac,su}$, $f_{h2,su}$) and 1 θ_B (i.e. $X_{ac,Batch7}$). In this study, only the θ_i showing IE $\leq$ 0.20 % were fixed at their initial values [Table 4] to enhance the capabilities of GSA and ABC for calibrating structured AD models, as mentioned in Section 2.3.4. The overall $J(\theta)$ variance explained by the GSA engine was around 70 % in all cases, confirming the validity of this methodology to assess the most influential θ in the HS-AD model (Oakley & O'Hagan, 2004).

IE provides a relative measure of the θ_i practical identifiability, while a high θ_i correlation – high difference between IE and GE – suggests that θ_i cannot be

independently calibrated with the available set of experimental data (Saltelli et al., 2006). As an example, GSA No. 1 showed that 40.7 % out of 72.4 % of the global *J(θ)* variance was explained by adding up the IE of 30 θ_P [Table 5], while the remaining 31.7 % variance was explained by correlations among these. For example, $k_{m,c4}$ explained individually around 4.4 % of the global variance (i.e. IE), though showing GE up to 17.9. This meant that the correlation of $k_{m,c4}$ with other θ was high, and any improvement in *J(θ)* obtained by solely modifying $k_{m,c4}$ could be partially or totally compensated by the modification of a correlated θ_i. In this line, the $k_{m,c4} \cdot f_{bu,bu}$ correlation in GSA No. 1 explained up to 2.8 % of the global variance (data not shown), due to the influence of $f_{bu,su}$ in *J(θ)* (i.e. IE = 2.0 % and GE = 24.4) [Table 5].

In this study, θ_i were disregarded by a single and low-demanding criterion (i.e. IE ≤ 0.20 %) [Table 5], since any chosen criterion for 'potential identifiability' would influence the GSA results when N ≥ 30. Meanwhile, GSA also depends on *N′* (i.e. ≤ 30) and/or the particular combination of θ_P and θ_B used. Thus, using a more demanding identifiability criterion (e.g. IE ≤ 0.50 % instead of 0.20 %) might have led to discard θ_i during preliminary GSA runs, which would be subsequently characterized as 'potentially identifiable'. For example, GSA No. 1 showed an IE = 0.22 % for $k_{m,c5}$, whereas GSA No. 7 eventually showed an IE = 0.67 % [Table 5]. To enhance identifiability, a strategy to reduce the gap between IE and GE for each θ_i is required (Kennedy & Petropoulos, 2017). However, reducing the IE to GE gap in this study would require to readapt the criterion used for 'potential identifiability'. One strategy might consist on fixing those θ_i showing, for example, IE ≤ 0.30 % in GSA No. 7 (i.e. $f_{ac,su}$), and then perform further rounds of GSA (i.e. GSA No. 8) until IE ~ GE for all θ_i.

With all the above, a second assessment for identifiability can be useful when using variance-based GSA for structured AD models. ABC is a well-suited tool in this regard, yielding also $p(\theta|y)$, in contrast to GSA. Importantly, both methodologies should yield equivalent results regarding the θ_i identifiability, though ABC is much computationally intensive than GSA, as explained in Section 3.2.1.

3.1.2. Importance of the $p(\theta)$ for Model Calibration

It must be noted that any $p(\theta)$ could be used to calibrate AD models, provided that θ do not contradict biochemical laws (e.g. $\theta_P \geq 0$ and $\theta_B \geq 0$) or disrupt mathematical resources (e.g. $pH_{UL,ac} > pH_{LL,ac}$) and the overall $p(\theta)$ range is as densely and homogeneously sampled as possible. On the other hand, the $p(\theta)$ distribution used (e.g. uniform, log-transformed uniform, normal) can be also crucial to determine $p(\theta|y)$ and the overall θ estimation.

In this study, using triplicates permitted to enhance the GSA representativeness (overall sampling) in presence of large N and $p(\theta)$ ranges. Meanwhile, a uniform distribution with mostly a 90 % modification was predefined for θ_P, whereas a log-transformed uniform distribution with a 50 % modification was allowed for θ_B [Table 4], as mentioned in Section 2.3.2. These specific $p(\theta)$ ranges were considered sufficiently wide for the objectives of this study, and were based mainly on experience and visual analysis of the overall model results. Particularly, the order of magnitude of many θ_P are relatively well characterized in literature according to their corresponding bio-physical-chemical meaning. Nonetheless, the order of magnitude of θ_B is highly unknown,

particularly after the inoculum centrifugation used in this study. Thus, using a uniform $p(\theta)$ permitted to emphasize the precision over punctual θ_P values within the $p(\theta_P)$ range, whereas the precision over the 'unknown' order of magnitude in the θ_B range was emphasized by using a log-transformed uniform distribution $p(log_{10}(\theta_B))$.

With all the above, using a different $p(\theta)$ range or distribution might alter the results of variance-based GSA and the overall calibration of structured AD models. For example, using considerably narrower $p(\theta_P)$ ranges in GSA No. 1 (i.e. $(1 - 0.3) \cdot \theta_{P,0} \leq \theta_P \leq (1 + 0.3) \cdot \theta_{P,0}$; *uniform* $p(\theta_P)$) resulted in some θ_P – which were highlighted as 'potentially identifiable' in this study – being disregarded as non-identifiable (e.g. $K_{h,pr}$ and $k_{m,c4}$), likely because part of their 'optimal' or 'sub-optimal' θ_P values were left outside the $p(\theta_P)$ range [Supplementary Information]. On the other hand, using wider ranges (i.e. $0.01 \cdot \theta_{P,0} \leq \theta_P \leq 3 \cdot \theta_{P,0}$; *uniform* $p(\theta_P)$), the results were not substantially different; i.e. only the $k_{m,c5}$ identifiability was additionally disregarded by GSA No. 1. However, using a log-transformed uniform distribution (i.e. $(1 + 0.5) \cdot log_{10}(\theta_{P,0}) \leq log_{10}(\theta_P) \leq (1 - 0.5) \cdot log10(\theta_{P,0})$; *uniform* $p(log_{10}(\theta_P))$) relatively altered the results of GSA No. 1; i.e. the order of magnitude of $k_{m,c5}$ and $k_{m,c4}$ was disregarded, while the order of magnitude of $K_{h,ch,slow}$ and $K_{S,Xh2}$ has was highlighted as highly important for the HS-AD model calibration. Therefore, for the correct calibration of structured AD models, both the $p(\theta)$ range and distribution should be set accordingly to all the prior information available for these θ, minimizing the $p(\theta)$ range explored alongside the number of simulations required for the objectives of the study.

3.1.3 Importance of the Available Data for Model Calibration

463 Provided the θ are structurally identifiable, practical identifiability relates to the quantity
464 as well as the quality (i.e. experimental errors and/or the sampling frequency) of the
465 experimental data available (Donoso-Bravo et al., 2011; Guisasola et al., 2006;
466 Nimmegeers et al., 2017; Rodriguez-Fernandez et al., 2006). Particularly, a reduced
467 number of experimental data associated to some model dynamics usually prevents
468 practical identifiability of the θ involved in these specific dynamics. For example, Y_b
469 might not be identifiable in AD models provided that the biomass concentration
470 dynamics were measured (Bernard et al., 2001).
471
472 In this study, the hydrolysis constant of readily-biodegradable carbohydrates ($K_{h,ch,fast}$)
473 and lipids ($K_{h,li}$), but also the maximum growth rate of sugar ($k_{m,su}$) and amino acid
474 ($k_{m,aa}$) degraders, showed a reduced influence in $J(\theta)$ by GSA. These results suggest that
475 either insufficient experimental data was available to calibrate $K_{h,ch,fast}$, $K_{h,li}$, $k_{m,su}$ and
476 $k_{m,aa}$, or that the biogas production in the HS-AD batch experiments [Table 1] was
477 mostly influenced by the VFA uptake – as the main limiting step. In the same line, due
478 to the Monod properties, k_m and K_S might be correlated when using batch experiments
479 for calibration (Dochain & Vanrolleghem, 2001; Flotats et al., 2010; Guisasola et al.,
480 2006). Nevertheless, GSA showed negligible influence for all K_S in this study, likely
481 due to using different batch experiments (i.e. ISR and TS) and/or a reduced number of
482 experimental data to obtain $J(\theta)$ [Equation 4].
483
484 The liquid-gas transfer coefficient (kLa) was also disregarded during the initial steps of
485 GSA (i.e. IE = 0.07 % and GE = 0.39) [Table 5]. The kLa coefficient is related to the
486 homogenization and mixing strategy, as well as other operational parameters in AD (e.g.

temperature and pH) (Batstone et al., 2002). In this study, all the HS-AD digesters were manually shaken. However, increasing the TS content can hamper the liquid-gas transfer mechanisms in HS-AD (Pastor-Poquet et al., 2019a). Therefore, a calibration strategy should be specifically envisaged to correctly calibrate kLa (e.g. using different stirring velocities/devices for mixing), since the presence of several θ in HS-AD models can prevent identifiability of kLa with the reduced number of experimental data usually available.

Importantly, both the NH_3 and H_2 inhibition parameters [Table 2] were shown as non-identifiable in this study, despite the strong influence of these parameters to regulate the biogas production in an ADM1-based model, as mentioned in Section 2.3.2. These results were associated to the reduced TAN and VFA dynamics in the experimental data, since only one single sacrifice experiment was available for calibration/validation. Therefore, despite using different initial conditions (i.e. ISR and/or TS) for model calibration, the NH_3 inhibition parameters in HS-AD of OFMSW cannot be assessed by using traditional batch experiments, where only the biogas production and composition are (usually) dynamically evaluated.

The above results condense the importance of an adequate sampling to enhance identifiability in AD models, but also to test hypotheses regarding the effects of inhibitory substances in HS-AD. Particularly, an extensive sampling for VFA, pH and TAN at different operational times during batch experiments is required to identify crucial parameters regarding the NH_3 inhibition in HS-AD of OFMSW. Therefore, sacrifice experiments and/or any sampling technique for batch setups – allowing the

thorough characterization of the reactor content variables in dynamic mode – should be recommended to calibrate structured HS-AD models using batch experiments. On the other hand, including (semi-)continuous datasets when available might also alleviate these identifiability issues during calibration (Bennett et al., 2013; Nimmegeers et al., 2017).

3.1.4 The Importance of Initial Conditions for Model Calibration

Interestingly, all θ_B except $X_{ac,Batch7}$ were shown as non-identifiable in this study [Table 5]. The reason presumably lies on the high k_m of all microorganisms 'shading' the effect of their initial concentration. For example, X_{pro} was associated to a maximum growth rate ($k_{m,pro}$) around 10 d^{-1} [Table 4]. Thus, X_{pro} doubles within 1 h (i.e. $\frac{\log(2)}{k_m} = \frac{\log(2) \cdot 24}{10} = 0.6\ h$), whereas the HS-AD batch experiments lasted considerably longer than 20 days [Table 1].

X_{ac} and X_{h2} are important variables to avoid batch acidification during the initial 0 - 10 days of HS-AD simulations, due to the rapid changes occurring in the bio-physical-chemistry during these days and the influence of these two microbial populations to define the buffering capacity (Batstone et al., 2002; Capson-Tojo et al., 2017). Nonetheless, these biomass concentrations were also rapidly disregarded by GSA in this study [Tables 3 and 4], except the 'potential identifiability' of $X_{ac,Batch7}$ suggested by GSA No. 7 which was likely explained by the influence of the order of magnitude of this particular biomass content to regulate the risk of acidification of the most extreme HS-AD condition in Experiment 7 (i.e. Batch No. 9, TS = 30 %) [Table 1].

With all the above, it is likely that only the initial biomass magnitude – not a precise value – was needed to calibrate the HS-AD model based on batch experiments. In other words, approximate biomass concentrations serve mainly to avoid acidification in HS-AD batch simulations, since these might not influence significantly the model calibration. The θ influence on $J(\theta)$ in this study was further assessed by ABC.

3.2 Parameter Optimization

3.2.1 Second Identifiability Assessment

Figure 1 shows $p(\theta'|y)$ using an $\varepsilon = 1.05$. The main statistics for these $p(\theta'|y)$ are summarized in Table 6, including the confidence ranges (i.e. 5 - 95 % interquartile range), since a reliable assessment of the θ confidence range is as important as the value of θ_{opt} themselves (Guisasola et al., 2006). The correlation matrix is included as Supplementary Information. Figure 2 shows the 5 - 95 % interquartile range *vs.* ε, since reducing progressively ε permitted to assess the convergence of the θ' posterior as second identifiability assessment.

Parameter identifiability is roughly associated to the 'sharpness' of the posterior distribution, $p(\theta|y)$ (Martin & Ayesa, 2010; Toni & Stumpf, 2010). In this line, $K_{h,pr}$, $K_{h,ch,slow}$, $k_{m,fa}$, $k_{m,c5}$, $k_{m,c4}$, $k_{m,ac}$, $pH_{LL,ac}$ and $f_{bu,su}$ showed relatively well-defined bell-shaped distributions by ABC, suggesting an adequate identifiability [Figure 1]. Meanwhile, $k_{m,pro}$, $k_{m,h2}$, k_d, $X_{ac,Batch7}$, $f_{ac,su}$ and $f_{h2,su}$ showed a more uniform-like distribution, suggesting a poorer identifiability. The substantial reduction observed in the interquartile range for $K_{h,pr}$, $K_{h,ch,slow}$, $k_{m,fa}$, $k_{m,c5}$, $k_{m,c4}$, $k_{m,ac}$, $pH_{LL,ac}$ and $f_{bu,su}$ (i.e. 60 - 80 %) corroborated their adequate identifiability in this study, in contrast to $k_{m,pro}$,

$k_{m,h2}$, k_d, $X_{ac,Batch7}$, $f_{ac,su}$ and $f_{h2,su}$ that showed a much constant interquartile range (i.e. ≤ 50 % reduction) [Figure 2]. The poor practical identifiability of these last θ' is explained by their high correlation with the rest of θ'. For example, the $f_{ac,su} \cdot f_{bu,su}$ correlation was -0.82, while $k_{m,pro} \cdot k_d$ was 0.72 – data not shown. As suggested in Section 3.1.4, $X_{ac,Batch7}$ served mainly to counteract the potential acidification in Batch No. 9, since the poor reduction in the interquartile range (i.e. 23 %) alongside the high correlation with other θ' (i.e. $pH_{LL,ac} \cdot X_{ac,Batch7} = 0.24$) indicated that only an approximate biomass content is needed to calibrate structured HS-AD models based on batch experiments.

As expected, ABC supported the identifiability assessment previously performed by GSA. In particular, θ' showing IE < 1.5 % in GSA No. 7 (i.e. $k_{m,pro}$, $k_{m,h2}$, and $f_{ac,su}$) [Table 5] were associated to a poor identifiability. However, some parameters showing an IE ≥ 1.5 % in GSA No. 7 (i.e. k_d, $X_{ac,Batch7}$ and $f_{h2,su}$) were also indicated as non-identifiable by ABC in contrast to GSA, suggesting that ABC was a more sensitive methodology for parameter identifiability in this study. With all the above, a more restrictive IE threshold (i.e. 0.50 % instead of 0.20 %) could have been used in further GSA rounds, once fixing poorly-identifiable parameters to any value within the prior, as mentioned in Section 3.1.1.

ABC is computationally intensive due to the high level of $J(\theta') - J_{min}(\theta') \leq \varepsilon$ rejection, particularly when using highly-demanding ε (Filippi et al., 2013; Toni & Stumpf, 2010). For example, the acceptance ratio was 0.129 when using ε = 1.80, meaning that only 1 out of 8 simulations was accepted for posterior evaluation, whereas the acceptance ratio was 0.004 when using ε = 1.10 – data not shown. Thus, ABC is not recommended to

assess identifiability in complex models with a large number of θ (i.e. $N \geq 30$). Different upgrades have been proposed to increase the ABC efficiency (Beaumont et al., 2009; Filippi et al., 2013; Toni & Stumpf, 2010), though the evaluation of these upgrades for calibrating structured AD models was out of the scope of this study. Conversely, the GSA engine relies upon a Bayesian emulator to speed up the analysis of model outputs (Kennedy & O'Hagan, 2001; Oakley & O'Hagan, 2004). Therefore, GSA can be an adequate tool to reduce the global computation required for parameter optimization, by preliminarily reducing the number of θ' to be further assessed by ABC as shown in this study.

3.2.2 Batch Simulations

Using the θ' mean as θ_{opt} [Table 6] led to a good approximation of both the methane production [Figure 3] and the rest of variables at the end of all batch experiments [Figure 4] used either for calibration (i.e. Batch No. 1, 3, 5, 6, 7 and 9) or cross-validation (i.e. Batch No. 2, 4 and 8) [Table 1]. Therefore, the θ' mean might be a good approximation of θ_{opt}, particularly for those θ' where practical identifiability was likely (i.e. $K_{h,pr}$, $K_{h,ch,slow}$, $k_{m,fa}$, $k_{m,c5}$, $k_{m,c4}$, $k_{m,ac}$, $pH_{LL,ac}$ and $f_{bu,su}$). Importantly, the HS-AD model was able to capture particularly well the TS and TAN contents, but also VS (data not shown), in all mono- and co-digestion experiments, confirming the suitability of the hypotheses used for the model development (Pastor-Poquet et al., 2018).

Some disagreements were also observed between the simulations and the experimental results. Particularly, the implementation of a reversible NH_3 inhibition function [Equation 1] in all the VFA and H_2 degrading populations [Table 2] was unable to

capture the VFA accumulation at the end of HS-AD experiments [Figure 4]. As the most noticeable example, calibration failed to represent the S_{bu} accumulation in Batch No. 6 [Figure 4e], yielding also a slight miss-adjustment in the methane production [Figure 3c]. More in general, S_{ac} and S_{bu} at the end of all experiments were poorly represented [Figure 4], despite the butyrate ($k_{m,c4}$) and acetate ($k_{m,ac}$) growth rates were adequately identified and the NH_3 inhibition upon the acetate uptake is a relatively well-established strategy in structured AD models (Batstone et al., 2002).

Two main reasons might explain the VFA disagreement between the model simulations and the experimental data available. The first reason relates to the relatively low amount of experimental data hampering calibration, as mentioned in Section 3.1.3. In this line, the NH_3 half-inhibition parameters in the VFA and/or H_2 uptakes ($K_{i,nh3}$) were disregarded as unimportant by GSA to represent the experimental data [Table 5], mainly because only Batch No. 1 contained the VFA, pH and TAN dynamics. The second reason relates to the poor suitability of the reversible non-competitive NH_3 inhibition function [Equation 1] to explain the VFA accumulation in HS-AD simulations, as discussed in next section.

3.3 Main Effects of Increasing the TS Content in HS-AD of OFMSW

In this study, calibration/cross-validation served to further test the hypotheses used for model construction (e.g. mass balances), particularly regarding the TS and VS simulation. Noteworthy, the correct simulation of TS is crucial in HS-AD, as TS determines the apparent concentration of soluble compounds subsequently affecting all the HS-AD bio-physical-chemical dynamics (Pastor-Poquet et al., 2019b). For example,

TS = 20 % supposes approximately 20 % higher apparent concentrations (i.e. kmol/kg H_2O) regarding the corresponding global concentrations (i.e. kmol/kg).

The HS-AD model was also calibrated/validated to assess the effects of increasing TS upon the NH_3 inhibition in HS-AD. Specifically, a high solute content – potentially associated to a high TS – exacerbates the solution 'non-ideality', affecting all the HS-AD dynamics (e.g. pH, NH_3 concentration, CO_2 transfer) (Pastor-Poquet et al., 2019b). More in detail, 'non-ideality' can lower S_{nh3}, serving as a potential source of NH_3 inhibition abatement in HS-AD of OFMSW. In this study, *I* ranged from 0.22 to 0.93 M [Figure 4c], emphasizing the need for an adequate 'non-ideal' bio-physical-chemical approach (Hafner & Bisogni, 2009; Solon et al., 2015). Importantly, despite the high *I* observed, S_{nh3} reached up to 0.13 mol N/kg in this study [Figure 4d] – equivalent to 0.16 mol N/kg H_2O (i.e. 2.3 g N/L). These S_{nh3} were considerably high, since reactors operated at $S_{nh3} \geq 1.0$ g N/L usually show an inefficient VFA conversion (Rajagopal et al., 2013).

The inefficient VFA conversion in HS-AD experiments was not well simulated by the reversible NH_3 inhibition function, as mentioned in Section 3.2.2. To understand the poor VFA simulation, it is necessary to consider the relatively flat inhibition described by Equation 1 but also the COD fluxes in the HS-AD model. Briefly, I_{nh3} is 0.50 when $S_{nh3,App} = K_{i,Snh3}$, whereas I_{nh3} is 0.33 when $S_{nh3,App} = 2 \cdot K_{i,Snh3}$ [Equation 1]. In other words, a non-competitive reversible inhibition by NH_3 might be far too 'blunt' to describe the actual effect of NH_3 upon the anaerobic biomass (Astals et al., 2018). On the other hand, due to the COD fractioning used in this study, approximately 54 % of

655 the COD from S_{su} [Table 6] and 26 % of the COD from S_{aa} flowed through the butyrate
656 pathway, whereas up to 80 % of the COD either from S_{su}, S_{aa} and/or long-chain fatty
657 acids (S_{fa}) flowed through the acetate pathway (Batstone et al., 2002). Meanwhile, a
658 considerable proportion of the initially biodegradable COD (i.e. 75 - 85 %) was
659 assigned to $X_{ch} + S_{su} + X_{pr} + S_{aa}$ [Table 3].
660
661 With all the above, the 'blunt' definition of the NH_3 inhibition function, alongside the
662 high COD flowing through the butyrate and acetate pathways, presumably favored the
663 X_{bu} and X_{ac} growth even at considerably high S_{nh3} (i.e. up to 2.3 g N/L) during
664 simulations. Summarizing, the high substrate content counterbalanced the effect of the
665 NH_3 inhibition, preventing the correct simulation of S_{bu} and S_{ac} accumulation at the end
666 of the HS-AD experiments. Therefore, the reversible non-competitive NH_3 inhibition
667 function [Equation 1] in the VFA and/or H_2 uptakes [Table 2] requires further testing to
668 represent the VFA accumulation observed in HS-AD of OFMSW. To this particular aim,
669 using extensive data regarding the VFA, pH and TAN dynamics in HS-AD simulations
670 is strongly recommended.
671
672 To end up, the HS-AD model (Pastor-Poquet et al., 2018) is a suitable platform to
673 understand the inner mechanisms of HS-AD, whereas further model developments
674 and/or model configurations (i.e. inhibition functions) should be also tested to enhance
675 our understanding about the VFA accumulation within HS-AD of OFMSW. Similarly,
676 additional experimental data is needed to thoroughly understand the role of NH_3
677 inhibition in HS-AD simulations. Specifically, extensive data regarding the main
678 species driving 'non-ideality' (i.e. VFA, pH, TAN) and/or further bio-physical-chemical

679 mechanisms (i.e. precipitation) in HS-AD seem to be crucial, due to the outstanding
680 importance of 'non-ideality' for the biochemical parameter optimization (Pastor-Poquet
681 et al., 2019b). In this scheme, the relatively simple calibration/validation methodology
682 presented in this study can serve to test the θ practical identifiability and confidence
683 ranges in presence of any set of experimental data and/or HS-AD model structure.
684
685
686 **4 CONCLUSIONS**
687 Nine different batch conditions were used to calibrate and cross-validate the HS-AD
688 model. For parameter optimization, variance-based GSA in tandem with ABC served to
689 evaluate the practical identifiability of 35 θ_P and 32 θ_B. Among all these, mostly 8 θ_P
690 were correctly identified with the available data, as corroborated by the convergence of
691 $p(\theta|y)$. The study also showed that HS-AD may be operated at $S_{nh3} \geq 2.3$ g N/L and $I \geq$
692 0.9 M, whereas a reversible non-competitive NH_3 inhibition function was not able to
693 explain the VFA accumulation in HS-AD of OFMSW. Therefore, further datasets about
694 the VFA, pH and TAN dynamics are required to enhance the θ practical identifiability,
695 whereas further model configurations should be tested to enhance the simulation of NH_3
696 inhibition in HS-AD.
697
698
699 **Acknowledgements**
700 This project has received funding from the European Union's Horizon 2020 research
701 and innovation programme under the Marie Sklodowska-Curie grant agreement No.

643071. Angela Andreella is gratefully acknowledged for revising all the statistical concepts.

REFERENCES

Astals, S., Peces, M., Batstone, D.J., Jensen, P.D., Tait, S. 2018. Characterising and modelling free ammonia and ammonium inhibition in anaerobic systems. *Water Res.*, **143**, 127-135.

Batstone, D.J., Keller, J., Angelidaki, I., Kalyuzhnyi, S.V., Pavlostathis, S.G., Rozzi, A., . . . Vavilin, V.A. 2002. The IWA Anaerobic Digestion Model No. 1 (ADM1). *Water Sci. Technol.*, **45**(10), 65-73.

Beaumont, M.A., Cornuet, J.-M., Marin, J.-M., Robert, C.P. 2009. Adaptive approximate Bayesian computation. *Biometrika*, **96**(4), 983-990.

Bennett, N.D., Croke, B.F.W., Guariso, G., Guillaume, J.H.A., Hamilton, S.H., Jakeman, A.J., . . . Andreassian, V. 2013. Characterising performance of environmental models. *Environ. Model. Software*, **40**, 1-20.

Bernard, O., Hadj-Sadok, Z., Dochain, D., Genovesi, A., Steyer, J.P. 2001. Dynamical model development and parameter identification for an anaerobic wastewater treatment process. *Biotechnol. Bioeng.*, **75**, 424-438.

Capson-Tojo, G., Trably, E., Rouez, M., Crest, M., Steyer, J.P., Delgenès, J.P., Escudié, R. 2017. Dry anaerobic digestion of food waste and cardboard at different substrate loads, solid contents and co-digestion proportions. *Bioresour. Technol.*, **233**, 166-175.

Dochain, D., Vanrolleghem, P. 2001. *Dynamical Modelling and Estimation in Wastewater Treatment Processes*. IWA Publishing, London, UK.

Donoso-Bravo, A., Mailier, J., Martin, C., Rodríguez, J., Aceves-Lara, C.A., Vande Wouwer, A. 2011. Model selection, identification and validation in anaerobic digestion: A review. *Water Res.*, **45**(17), 5347-5364.

Filippi, S., Barnes, C.P., Cornebise, J., Stumpf, M.P. 2013. On optimality of kernels for approximate Bayesian computation using sequential Monte Carlo. *Stat. Appl. Genet. Mol. Biol.*, **12**(1), 87–107.

Flotats, X., Ahring, B.K., Angelidaki, I. 2003. Parameter identification of thermophilic anaerobic degradation of valerate. *Appl. Biochem. Biotechnol.*, **109**(1-3), 47-62.

Flotats, X., Palatsi, J., Fernandez, B., Colomer, M.A., Illa, J. 2010. Identifying anaerobic digestion models using simultaneous batch experiments. *Environ. Engineer. Manag. J.*, **9**(3), 313-318.

Garcia-Gen, S., Sousbie, P., Rangaraj, G., Lema, J.M., Rodriguez, J., Steyer, J.P., Torrijos, M. 2015. Kinetic modelling of anaerobic hydrolysis of solid wastes, including disintegration processes. *Waste Manage.*, **35**, 96-104.

Guisasola, A., Baeza, J.A., Carrera, J., Sin, G., Vanrolleghem, P.A., Lafuente, J. 2006. The influence of experimental data quality and quantity on parameter estimation accuracy: Andrews inhibition model as a case study. *Educ. Chem. Eng.*, **1**(1), 139-145.

Hafner, S.D., Bisogni, J.J. 2009. Modeling of ammonia speciation in anaerobic digesters. *Water Res.*, **43**(17), 4105-4114.

Kennedy, M.C., O'Hagan, A. 2001. Bayesian calibration of computer models. *J. Roy. Stat. Soc. Ser. B. (Stat. Method.)*, **63**(3), 425-464.

Kennedy, M.C., Petropoulos, G.P. 2017. GEM-SA: The gaussian emulation machine for sensitivity analysis. in: *Sensitivity Analysis in Earth Observation Modelling*, (Ed.) G.P. Petropoulos, Elsevier. Amsterdam, Netherlands.

Martin, C., Ayesa, E. 2010. An Integrated Monte Carlo Methodology for the calibration of water quality models. *Ecol. Model.*, **221**(22), 2656-2667.

Nimmegeers, P., Lauwers, J., Telen, D., Logist, F., Impe, J.V. 2017. Identifiability of large-scale non-linear dynamic network models applied to the ADM1-case study. *Math. Biosci.*, **288**, 21-34.

Nott, D.J., Marshall, L., Brown, J. 2012. Generalized likelihood uncertainty estimation (GLUE) and approximate Bayesian computation: What's the connection? *Water Resour. Res.*, **48**(12).

Oakley, J.E., O'Hagan, A. 2004. Probabilistic sensitivity of complex models: A Bayesian approach. *J. Roy. Stat. Soc. Ser. B. (Stat. Method.)*, **66**(3), 751-769.

Pastor-Poquet, V., Papirio, S., Steyer, J.-P., Trably, E., Escudié, R., Esposito, G. 2018. High-solids anaerobic digestion model for homogenized reactors. *Water Res.*, **142**, 501-511.

Pastor-Poquet, V., Papirio, S., Trably, E., Rintala, J., Escudié, R., Esposito, G. 2019a. High-Solids Anaerobic Digestion requires a tradeoff between Total Solids, Inoculum-to-Substrate Ratio and Ammonia Inhibition. *Int. J. Environ. Sci. Technol.*, 1-15.

Pastor-Poquet, V., Papirio, S., Steyer, J.-P., Trably, E., Escudié, R., Esposito, G. 2019b. Modelling Non-Ideal Bio-Physical-Chemical Effects on High-Solids Anaerobic Digestion of the Organic Fraction of Municipal Solid Waste. *J. Environ. Manage.*, **238**, 408-419.

Rajagopal, R., Masse, D.I., Singh, G. 2013. A critical review on inhibition of anaerobic digestion process by excess ammonia. *Bioresour. Technol.*, **143**, 632-641.

Ratto, M., Tarantola, S., Saltelli, A. 2001. Sensitivity analysis in model calibration: GSA-GLUE approach. *Comput. Phys. Commun.*, **136**, 212-224.

Rodriguez-Fernandez, M., Egea, J.A., Banga, J.R. 2006. Novel metaheuristic for parameter estimation in nonlinear dynamic biological systems. *BMC Bioinformatics*, **7**, 483.

Saltelli, A., Ratto, M., Tarantola, S., Campolongo, F. 2006. Sensitivity analysis practices: Strategies for model-based inference. *Reliab. Eng. Syst. Saf.*, **91**(10-11), 1109-1125.

Solon, K., Flores-Alsina, X., Mbamba, C.K., Volcke, E.I., Tait, S., Batstone, D., . . . Jeppsson, U. 2015. Effects of ionic strength and ion pairing on (plant-wide) modelling of anaerobic digestion. *Water Res.*, **70**, 235-245.

Toni, T., Stumpf, M.P. 2010. Simulation-based model selection for dynamical systems in systems and population biology. *Bioinformatics*, **26**(1), 104-110.

TABLE CAPTIONS

Table 1. Batch experiments and initial conditions used for HS-AD model calibration and cross-validation

Table 2. Biochemical rates used for the HS-AD model in this study

Table 3. Initial conditions used for all batch simulations in this study

Table 4. Main input parameters (θ) used for global sensitivity analysis (GSA), including the initial values, lower and upper thresholds

Table 5. Global sensitivity analysis (GSA) of input parameters (θ): Individual (IE) and global (GE) effects upon the objective function, $J(\theta)$, variance

Table 6. Calibration of potentially-identifiable input parameters (θ'): Prior and posterior distributions

805 **FIGURE CAPTIONS**
806
807 **Figure 1**. Posterior parameter distribution using 400 simulations and $\varepsilon = 1.05$
808 **Figure 2**. Interquartile range (percentiles 5 to 95 %) of the posterior parameter
809 distribution using $\varepsilon \geq 1.05$ and $\varepsilon \leq 2.50$
810 **Figure 3**. Methane production with mono-digestion of dried OFMSW at a) ISR = 1.00;
811 b) ISR = 1.50; and c) ISR = 1.00; and co-digestion of dried OFMSW and sawdust at d)
812 ISR = 0.16. Dots represent experimental data, while lines represent simulated values.
813 **Figure 4**. Main variables at the end of the four batch experiments: a) Total solids (TS);
814 b) total ammonia nitrogen (TAN, S_{in}); c) ionic strength (I); d) free ammonia nitrogen
815 (NH_3, S_{nh3}); e) acetic acid (S_{ac}); f) propionic acid (S_{pro}); g) butyric acid (S_{bu}); and h)
816 valeric acid (S_{va}). Crosses represent experimental data, while geometries represent
817 simulated values
818
819

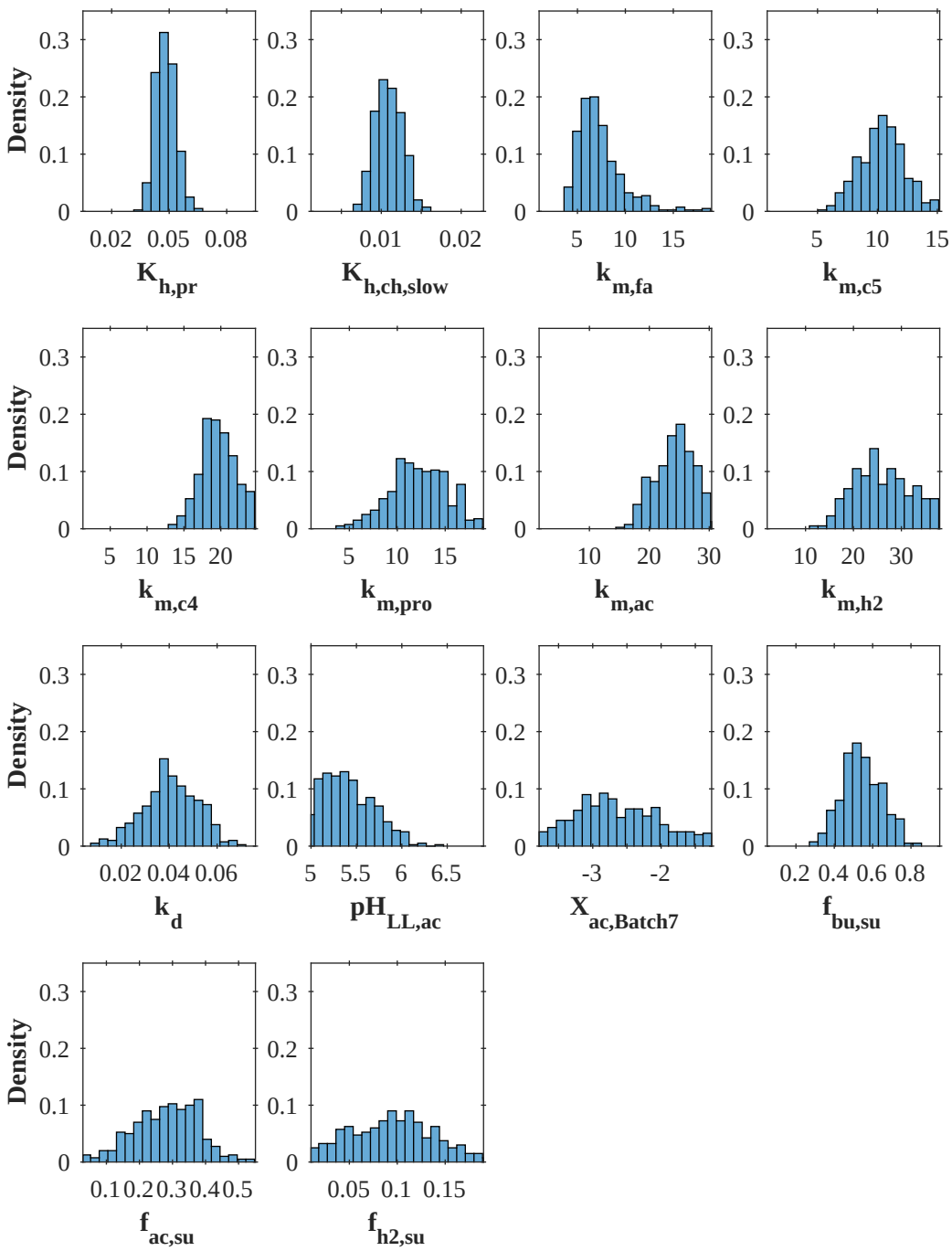

Figure 1. Posterior parameter distributions using 400 simulations and ε = 1.05

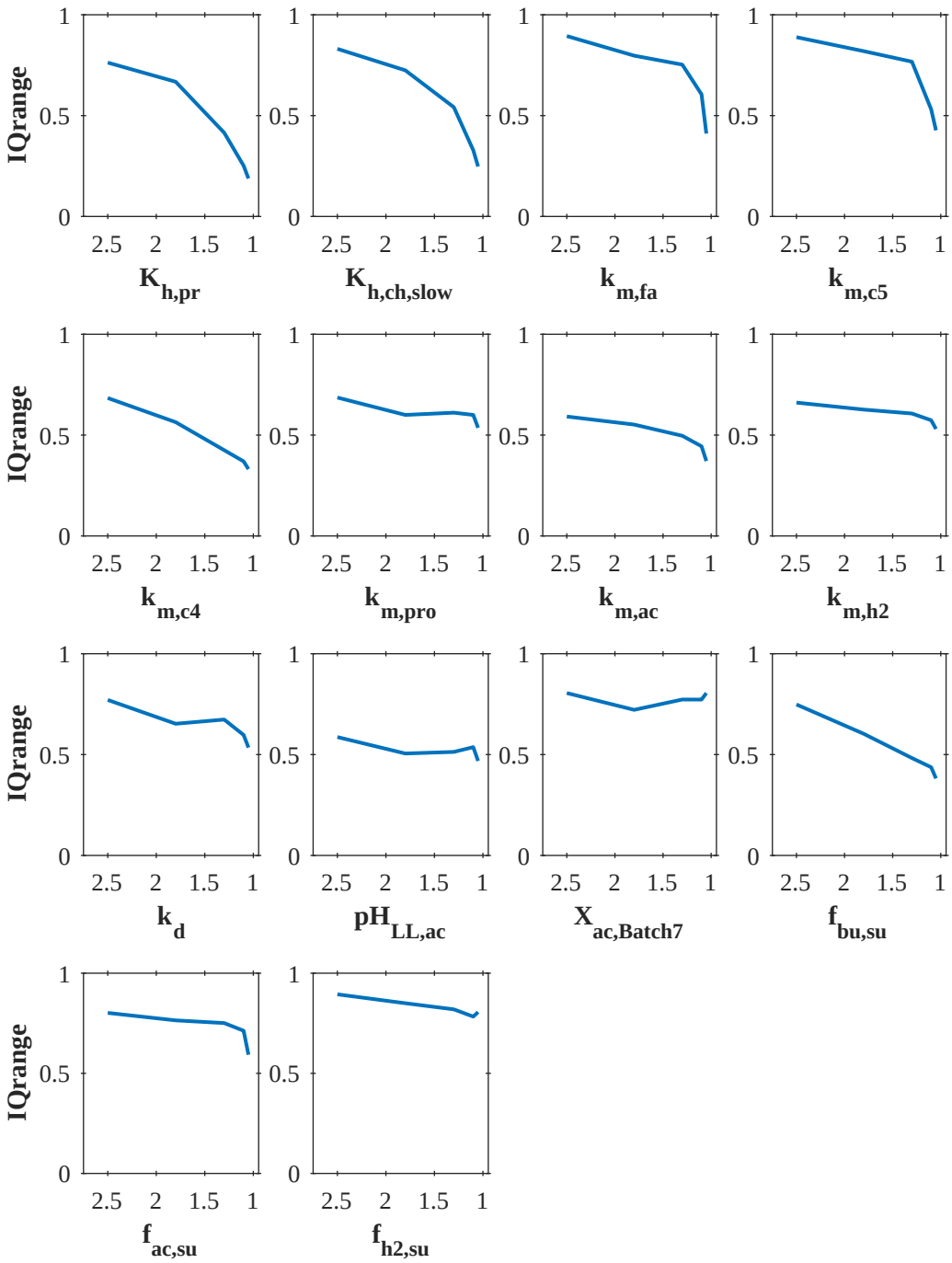

Figure 2. Interquartile range (percentiles 5 to 95 %) of the posterior parameter distributions using $\varepsilon \geq 1.05$ and $\varepsilon \leq 2.50$

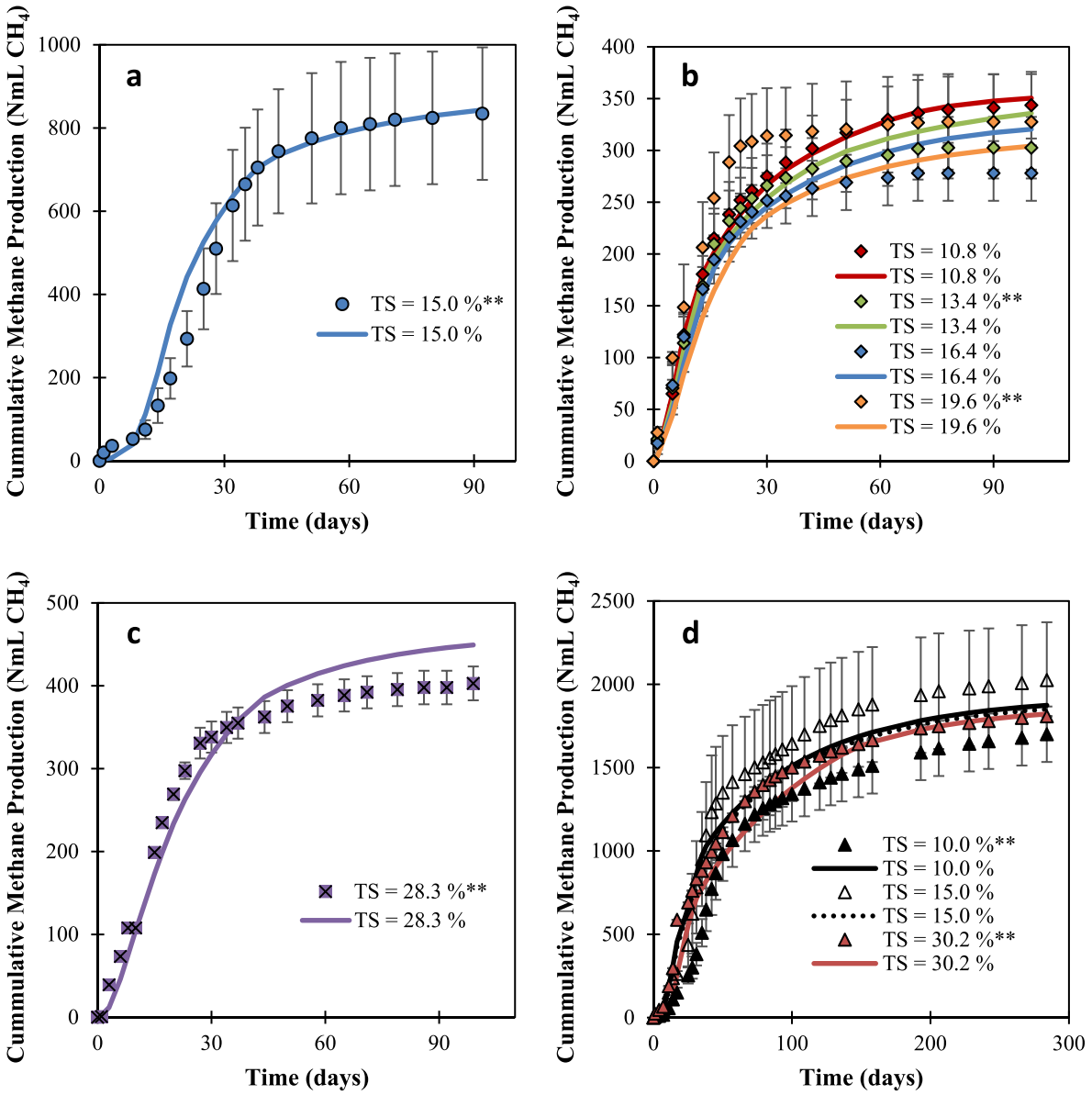

Figure 3. Methane production with mono-digestion of dried OFMSW at a) ISR = 1.00; b) ISR = 1.50; and c) ISR = 1.00; and co-digestion of dried OFMSW and sawdust at d) ISR = 0.16. Dots represent experimental data, while lines represent simulated values.
**Experimental data used for calibration

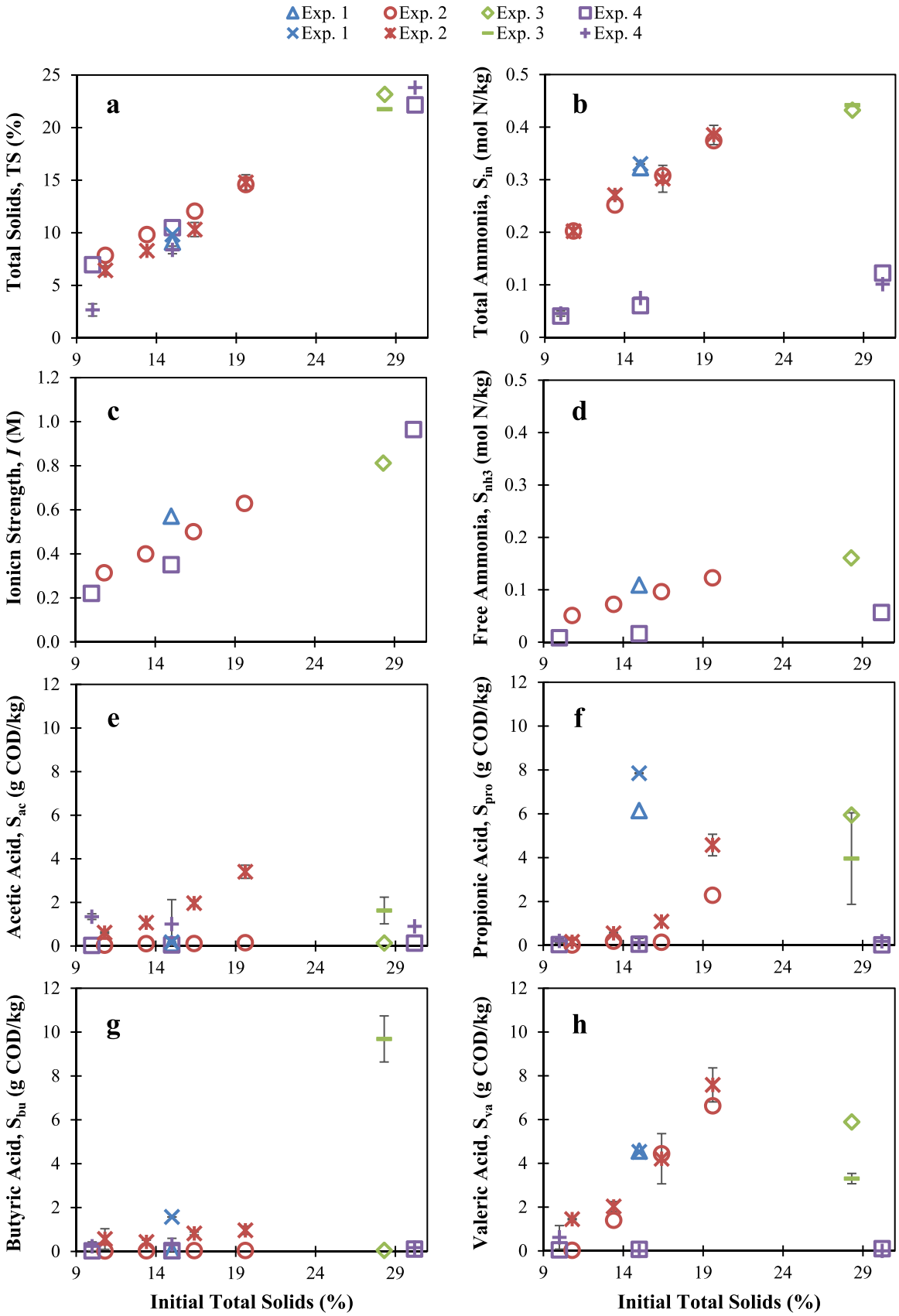

Figure 4. Main variables at the end of the four batch experiments: a) Total solids (TS); b) total ammonia nitrogen (TAN, S_{in}); c) ionic strength (I); d) free ammonia nitrogen (NH_3, S_{nh3}); e) acetic acid (S_{ac}); f) propionic acid (S_{pro}); g) butyric acid (S_{bu}); and h) valeric acid (S_{va}). Crosses represent experimental data, while geometries represent simulated values

Table 1. Batch experiments and initial conditions used for HS-AD model calibration and cross-validation

Substrate	Exp. No.	Batch No.	ISR (g VS/g VS)	Initial TS (%)	No. Replicates	Design Volume (mL)	Exp. Time (days)	Calibration or Validation
OFMSW	**1**	1	1.00	15.0	15	280	92	C
	2	2	1.50	10.8	3	160	100	V
		3		13.4	3			C
		4		16.4	3			V
		5		19.6	3			C
	3	6	0.50	28.3	2	280	99	C
OFMSW + Sawdust	**4**	7	0.16	10.0	3	280	284	C
		8		15.0	2			V
		9		30.2	1			C

Table 2. Biochemical rates used for the HS-AD model in this study

Process	Rate (r_j, kgCOD m^{-3} d^{-1})
Hydrolysis of Fast Biodegradable Carbohydrates	$k_{h,ch,fast} \cdot X_{ch,fast}$
Hydrolysis of Slow Biodegradable Carbohydrates	$k_{h,ch,slow} \cdot X_{ch,slow}$
Hydrolysis of Proteins	$k_{h,pr} \cdot X_{pr}$
Hydrolysis of Lipids	$k_{h,li} \cdot X_{li}$
Sugars Uptake	$k_{m,su} \cdot S_{su,App}/(K_{S,Xsu}+S_{su,App}) \cdot X_{su} \cdot I_{pH} \cdot I_{in}$
Aminoacids Uptake	$k_{m,aa} \cdot S_{aa,App}/(K_{S,Xaa}+S_{aa,App}) \cdot X_{aa} \cdot I_{pH} \cdot I_{in}$
LCFA Uptake	$k_{m,fa} \cdot S_{fa}/(K_{S,Xfa}+S_{fa}) \cdot X_{fa} \cdot I_{pH} \cdot I_{in} \cdot I_{h2}$
Valerate Uptake	$k_{m,c5} \cdot S_{va,App}/(K_{S,Xc5}+S_{va,App}) \cdot X_{c5} \cdot I_{pH} \cdot I_{in} \cdot I_{h2} \cdot I_{nh3}$
Butyrate Uptake	$k_{m,c4} \cdot S_{bu,App}/(K_{S,Xc4}+S_{bu,App}) \cdot X_{c4} \cdot I_{pH} \cdot I_{in} \cdot I_{h2} \cdot I_{nh3}$
Propionate Uptake	$k_{m,pro} \cdot S_{pro,App}/(K_{S,Xpro}+S_{pro,App}) \cdot X_{pro} \cdot I_{pH} \cdot I_{in} \cdot I_{h2} \cdot I_{nh3}$
Acetate Uptake	$k_{m,ac} \cdot S_{ac,App}/(K_{S,Xac}+S_{ac,App}) \cdot X_{ac} \cdot I_{pH} \cdot I_{in} \cdot I_{nh3}$
Hydrogen Uptake	$k_{m,h2} \cdot S_{h2,App}/(K_{S,Xh2}+S_{h2,App}) \cdot X_{h2} \cdot I_{pH} \cdot I_{in} \cdot I_{nh3}$
Sugar Degraders Decay	$k_d \cdot X_{su}$
Aminoacids Degraders Decay	$k_d \cdot X_{aa}$
LCFA Degraders Decay	$k_d \cdot X_{fa}$
Valerate Degraders Decay	$k_d \cdot X_{c5}$
Butyrate Degraders Decay	$k_d \cdot X_{c4}$
Propionate Degraders Decay	$k_d \cdot X_{pro}$
Acetate Degraders Decay	$k_d \cdot X_{ac}$
Hydrogen Degraders Decay	$k_d \cdot X_{h2}$

with

$I_{in} = S_{in,App}/(K_{i,Sin} + S_{in,App})$

$I_{h2} = K_{i,Sh2}/(K_{i,Sh2} + S_{h2,App})$

$I_{pH} = K_{pH}\text{^}N_{pH}/(K_{pH}\text{^}N_{pH} + S_{h+}\text{^}N_{pH})$

$I_{nh3} = K_{i,Snh3}/(K_{i,Snh3} + S_{nh3,App})$

Table 3. Initial conditions used for all batch simulations in this study

Name	Mono-digestion						Co-digestion			Units
	ISR = 1.00	ISR = 1.50				ISR = 0.50	ISR = 0.16			
	TS=15.0%	TS=9.5%	TS=13.5%	TS=16.5%	TS=19.4%	TS=28.3%	TS=10.0%	TS=15.0%	TS=30.2%	
S_{su}	9.761	6.920	8.776	10.861	13.245	6.201	1.800	2.779	6.496	kg COD m^{-3}
S_{aa}	3.187	5.856	7.346	9.099	11.201	7.679	0.972	1.503	3.571	kg COD m^{-3}
S_{fa}	2.610	1.656	2.186	2.702	3.184	1.467	0.377	0.579	1.300	kg COD m^{-3}
S_{va}	0.791	1.015	1.282	1.582	1.936	1.061	1.467	2.269	5.314	kg COD m^{-3}
S_{bu}	0.500	0.195	0.244	0.302	0.370	1.518	0.230	0.355	0.831	kg COD m^{-3}
S_{pro}	2.059	0.877	1.109	1.368	1.674	2.565	1.367	2.115	4.952	kg COD m^{-3}
S_{ac}	0.103	0.035	0.044	0.054	0.066	0.871	0.058	0.090	0.210	kg COD m^{-3}
S_{h2}	1.00E-08	1.00E-08	1.00E-08	1.00E-08	1.00E-08	1.00E-08	1.00E-08	1.00E-08	1.00E-08	kg COD m^{-3}
S_{ch4}	1.00E-08	1.00E-08	1.00E-08	1.00E-08	1.00E-08	1.00E-08	1.00E-08	1.00E-08	1.00E-08	kg COD m^{-3}
S_{ic}	0.029	0.014	0.017	0.021	0.026	0.037	0.008	0.013	0.030	kmol C m^{-3}
S_{in}	0.186	0.125	0.157	0.194	0.238	0.229	0.033	0.051	0.120	kmol N m^{-3}
S_i	1.00E-08	1.00E-08	1.00E-08	1.00E-08	1.00E-08	1.00E-08	1.00E-08	1.00E-08	1.00E-08	kg COD m^{-3}
$S_{i,subs}$	34.706	29.233	37.076	45.883	55.954	90.351	27.565	42.559	99.486	kgCOD m^{-3}
$X_{ch,fast}$	29.283	13.840	17.553	21.722	26.490	31.003	5.400	8.337	19.489	kg COD m^{-3}
$X_{ch,slow}$	-	-	-	-	-	-	27.360	42.242	98.743	kg COD m^{-3}
X_{pr}	28.680	11.713	14.692	18.197	22.402	38.393	5.834	9.016	21.425	kg COD m^{-3}
X_g	18.271	3.312	4.373	5.405	6.367	5.866	2.637	4.053	9.102	kg COD m^{-3}
X_{su} (*)	0.050	0.050	0.063	0.078	0.095	0.150	0.005	0.008	0.018	kg COD m^{-3}
X_{aa} (*)	0.050	0.050	0.063	0.078	0.095	0.060	0.005	0.008	0.018	kg COD m^{-3}
X_{fa} (*)	0.010	0.020	0.025	0.031	0.038	0.030	0.001	0.001	0.002	kg COD m^{-3}
X_{c5} (*)	0.005	0.010	0.013	0.016	0.019	0.030	0.001	0.001	0.002	kgCOD m^{-3}
X_{c4} (*)	0.001	0.050	0.063	0.078	0.095	0.030	0.001	0.001	0.002	kg COD m^{-3}
X_{pro} (*)	0.005	0.020	0.025	0.031	0.038	0.030	0.001	0.001	0.003	kg COD m^{-3}
X_{ac} (*)	0.024	0.150	0.190	0.234	0.286	0.100	0.003**	0.005	0.011	kg COD m^{-3}
X_{h2} (*)	0.050	0.200	0.253	0.312	0.382	0.090	0.003	0.005	0.011	kg COD m^{-3}
X_i	1.00E-08	1.00E-08	1.00E-08	1.00E-08	1.00E-08	1.00E-08	1.00E-08	1.00E-08	1.00E-08	kg COD m^{-3}
$X_{i,subs}$	86.765	73.083	92.689	114.706	139.885	225.877	68.914	106.398	248.714	kg COD m^{-3}
S_{cat}	0.100	0.060	0.075	0.091	0.109	0.166	0.040	0.059	0.120	kmoleq m^{-3}
S_{an}	0.051	0.040	0.050	0.060	0.073	0.069	0.020	0.030	0.060	kmoleq m^{-3}
M_{Global}	37.12	29.92	24.02	19.80	16.47	23.45	138.23	93.13	46.13	g
ρ_{Global}	1078	1059	1075	1093	1113	1128	1088	1134	1316	kg m^{-3}
TS	15.0	10.8	13.4	16.4	19.6	28.3	10.0	15.0	30.2	%
VS	12.4	9.1	11.4	13.9	16.6	24.0	9.6	14.2	28.6	%
$N_{i,subs}$	0.0010	0.0012	0.0012	0.0012	0.0012	0.0010	0.0004	0.0004	0.0004	kmol N kg COD^{-1}
$V_{Reactor}$	280	160	160	160	160	280	160	160	160	mL

** These values were assessed by Global Sensitivity Analysis (GSA). ** This value was also assessed by Approximate Bayesian Computation (ABC). The inoculum-to-substrate ratio (ISR) is expressed in g VS/g VS*

Table 4. Main input parameters (θ) used for global sensitivity analysis (GSA), including the initial values, lower and upper thresholds

Model Parameter	Units	ADM1	Initial Value	Lower Threshold	Upper Threshold	Initial Concentration	Units	Initial Value*	Lower Threshold*	Upper Threshold*
$K_{h,ch,fast}$	d^{-1}	10	0.120	0.012	0.228	$X_{su,Batch1}$	kg COD m^{-3}	-1.301	-1.952	-0.651
$K_{h,pr}$	d^{-1}	10	0.050	0.005	0.095	$X_{su,Batch2}$	kg COD m^{-3}	-1.301	-1.952	-0.651
$K_{h,li}$	d^{-1}	10	0.080	0.008	0.152	$X_{su,Batch6}$	kg COD m^{-3}	-0.824	-1.236	-0.412
$K_{h,ch,slow}$	d^{-1}	-	0.012	0.001	0.023	$X_{su,Batch7}$	kg COD m^{-3}	-2.301	-3.452	-1.151
$k_{m,su}$	d^{-1}	70	70	7	133	$X_{aa,Batch1}$	kg COD m^{-3}	-1.301	-1.952	-0.651
$k_{m,aa}$	d^{-1}	70	70	7	133	$X_{aa,Batch2}$	kg COD m^{-3}	-1.301	-1.952	-0.651
$k_{m,fa}$	d^{-1}	10	10	1	19	$X_{aa,Batch6}$	kg COD m^{-3}	-1.222	-1.833	-0.611
$k_{m,c5}$	d^{-1}	30	8	1	15	$X_{aa,Batch7}$	kg COD m^{-3}	-2.301	-3.452	-1.151
$k_{m,c4}$	d^{-1}	30	13	1	25	$X_{fa,Batch1}$	kg COD m^{-3}	-2.000	-3.000	-1.000
$k_{m,pro}$	d^{-1}	20	10	1	19	$X_{fa,Batch2}$	kg COD m^{-3}	-1.699	-2.548	-0.849
$k_{m,ac}$	d^{-1}	16	16	2	30	$X_{fa,Batch6}$	kg COD m^{-3}	-1.523	-2.284	-0.761
$k_{m,h2}$	d^{-1}	35	20	2	38	$X_{fa,Batch7}$	kg COD m^{-3}	-3.301	-4.952	-1.651
k_d	d^{-1}	0.040	0.040	0.004	0.076	$X_{c5,Batch1}$	kg COD m^{-3}	-2.301	-3.452	-1.151
$K_{S,Xsu}$	kg COD m^{-3}	1.00	1.00	0.1	1.9	$X_{c5,Batch2}$	kg COD m^{-3}	-2.000	-3.000	-1.000
$K_{S,Xaa}$	kg COD m^{-3}	0.30	0.30	0.03	0.57	$X_{c5,Batch6}$	kg COD m^{-3}	-1.523	-2.284	-0.761
$K_{S,Xfa}$	kg COD m^{-3}	0.40	0.40	0.04	0.76	$X_{c5,Batch7}$	kg COD m^{-3}	-3.222	-4.833	-1.611
$K_{S,Xc5}$	kg COD m^{-3}	0.40	0.40	0.04	0.76	$X_{c4,Batch1}$	kg COD m^{-3}	-3.000	-4.500	-1.500
$K_{S,Xc4}$	kg COD m^{-3}	0.40	0.40	0.04	0.76	$X_{c4,Batch2}$	kg COD m^{-3}	-1.301	-1.952	-0.651
$K_{S,Xpro}$	kg COD m^{-3}	0.30	0.30	0.03	0.57	$X_{c4,Batch6}$	kg COD m^{-3}	-1.523	-2.284	-0.761
$K_{S,Xac}$	kg COD m^{-3}	0.30	0.30	0.03	0.57	$X_{c4,Batch7}$	kg COD m^{-3}	-3.222	-4.833	-1.611
$K_{S,Xh2}$	kg COD m^{-3}	5.00E-05	5.00E-05	0.000005	0.000095	$X_{pro,Batch1}$	kg COD m^{-3}	-2.301	-3.452	-1.151
$pH_{LL,ac}$	-	6.00	5.80	5.00	6.90	$X_{pro,Batch2}$	kg COD m^{-3}	-1.699	-2.548	-0.849
$K_{i,Snh3,Xc5}$	kmol N m^{-3}	-	0.0070	0.0007	0.0133	$X_{pro,Batch6}$	kg COD m^{-3}	-1.523	-2.284	-0.761
$K_{i,Snh3,Xc4}$	kmol N m^{-3}	-	0.0100	0.0010	0.0190	$X_{pro,Batch7}$	kg COD m^{-3}	-3.097	-4.645	-1.548
$K_{i,Snh3,Xpro}$	kmol N m^{-3}	-	0.0100	0.0010	0.0190	$X_{ac,Batch1}$	kg COD m^{-3}	-1.620	-2.430	-0.810
$K_{i,Snh3,Xac}$	kmol N m^{-3}	0.0110	0.0040	0.0004	0.0076	$X_{ac,Batch2}$	kg COD m^{-3}	-0.824	-1.236	-0.412
$K_{i,Snh3,Xh2}$	kmol N m^{-3}	-	0.0150	0.0015	0.0285	$X_{ac,Batch6}$	kg COD m^{-3}	-1.000	-1.500	-0.500
$f_{bu,su}$	kg COD kg COD^{-1}	0.130	0.500	0.050	0.950	$X_{ac,Batch7}$	kg COD m^{-3}	-2.523	-3.784	-1.261
$f_{ac,su}$	kg COD kg COD^{-1}	0.270	0.290	0.029	0.551	$X_{h2,Batch1}$	kg COD m^{-3}	-1.301	-1.952	-0.651
$f_{h2,su}$	kg COD kg COD^{-1}	0.190	0.100	0.010	0.190	$X_{h2,Batch2}$	kg COD m^{-3}	-0.699	-1.048	-0.349
$K_{i,Sh2,Xfa}$	kg COD m^{-3}	3.00E-05	1.00E-05	1.00E-06	1.90E-05	$X_{h2,Batch6}$	kg COD m^{-3}	-1.046	-1.569	-0.523
$K_{i,Sh2,Xc5}$	kg COD m^{-3}	3.00E-05	3.00E-05	3.00E-06	5.70E-05	$X_{h2,Batch7}$	kg COD m^{-3}	-2.523	-3.784	-1.261
$K_{i,Sh2,Xc4}$	kg COD m^{-3}	3.00E-05	3.00E-05	3.00E-06	5.70E-05	-	-	-	-	
$K_{i,Sh2,Xpro}$	kg COD m^{-3}	1.00E-05	1.00E-05	1.00E-06	1.90E-05	-	-	-	-	
k_La	d^{-1}	200	200	20	380	-	-	-	-	

* *Logarithm-transformed:* $log_{10}(\theta_B)$

Table 5. Global sensitivity analysis (GSA) of input parameters (θ): Individual (IE) and global (GE) effects upon the objective function, $J(\theta)$, variance

GSA No.1			GSA No.2			GSA No.3			GSA No.4			GSA No.5			GSA No.6			GSA No.7		
θ	IE (%)	GE	θ	IE (%)	GE	θ	IE (%)	GE	θ	IE (%)	GE	θ	IE (%)	GE	θ	IE (%)	GE	θ	IE (%)	GE
$K_{h,ch,fast}$	0.08	0.63	$K_{h,pr}$	1.75	5.23	$K_{h,pr}$	2.75	8.62	$K_{h,pr}$	2.21	7.33	$K_{h,pr}$	1.01	5.42	$K_{h,pr}$	2.00	10.44	$K_{h,pr}$	1.97	7.72
$K_{h,pr}$	2.01	7.56	$K_{h,li}$	0.25	0.69	$K_{h,li}$	0.26	2.54	$K_{h,li}$	0.11	2.85	$K_{h,ch,slow}$	4.28	14.61	$K_{h,ch,slow}$	4.07	14.47	$K_{h,ch,slow}$	4.43	17.86
$K_{h,li}$	0.29	2.07	$K_{h,ch,slow}$	5.87	16.21	$K_{h,ch,slow}$	5.83	14.32	$K_{h,ch,slow}$	5.22	16.59	$k_{m,fa}$	0.46	4.14	$k_{m,fa}$	1.15	5.66	$k_{m,fa}$	1.11	8.95
$K_{h,ch,slow}$	6.45	17.27	$k_{m,aa}$	0.07	0.43	$k_{m,fa}$	1.21	7.25	$k_{m,fa}$	0.56	4.81	$k_{m,c5}$	0.22	1.63	$k_{m,c5}$	1.59	8.34	$k_{m,c5}$	0.67	5.72
$k_{m,su}$	0.16	3.82	$k_{m,fa}$	0.81	5.97	$k_{m,c5}$	0.80	3.12	$k_{m,c5}$	0.73	3.31	$k_{m,c4}$	1.38	11.18	$k_{m,c4}$	1.50	13.79	$k_{m,c4}$	2.39	15.94
$k_{m,aa}$	0.53	2.43	$k_{m,c5}$	0.33	1.49	$k_{m,c4}$	2.23	17.17	$k_{m,c4}$	2.47	19.12	$k_{m,pro}$	1.77	8.66	$k_{m,pro}$	1.23	11.37	$k_{m,pro}$	0.72	9.24
$k_{m,fa}$	0.91	4.34	$k_{m,c4}$	2.12	12.96	$k_{m,pro}$	0.51	8.59	$k_{m,pro}$	0.75	10.21	$k_{m,ac}$	3.56	12.26	$k_{m,ac}$	5.11	17.49	$k_{m,ac}$	4.13	17.22
$k_{m,c5}$	0.22	3.64	$k_{m,pro}$	0.44	10.49	$k_{m,ac}$	7.18	17.17	$k_{m,ac}$	4.67	11.62	$k_{m,h2}$	3.72	13.46	$k_{m,h2}$	4.13	15.65	$k_{m,h2}$	1.46	12.35
$k_{m,c4}$	4.39	17.87	$k_{m,ac}$	3.16	10.71	$k_{m,h2}$	4.07	10.68	$k_{m,h2}$	3.57	11.84	k_d	5.16	15.78	k_d	3.37	9.47	k_d	4.43	13.37
$k_{m,pro}$	0.62	8.62	$k_{m,h2}$	2.60	8.32	k_d	3.67	9.00	k_d	3.22	8.23	$K_{S,Xh2}$	0.13	1.09	$pH_{LL,ac}$	10.24	24.61	$pH_{LL,ac}$	11.69	29.21
$k_{m,ac}$	4.88	16.35	k_d	2.86	7.83	$K_{S,Xh2}$	0.40	1.76	$K_{S,Xh2}$	0.22	0.91	$pH_{LL,ac}$	11.04	25.72	$f_{bu,su}$	3.34	26.74	$f_{bu,su}$	1.89	24.59
$k_{m,h2}$	1.60	11.78	$K_{S,Xh2}$	0.71	2.03	$pH_{LL,ac}$	11.09	22.10	$pH_{LL,ac}$	9.69	18.95	$K_{i,Snh3,Xh2}$	0.21	3.16	$f_{ac,su}$	0.96	13.49	$f_{ac,su}$	0.22	9.58
k_d	1.65	5.26	$pH_{LL,ac}$	11.48	25.57	$K_{i,Snh3,Xh2}$	0.32	2.61	$K_{i,Snh3,Xh2}$	0.39	1.91	$f_{bu,su}$	4.03	30.77	$f_{h2,su}$	5.00	14.87	$f_{h2,su}$	6.37	19.92
$K_{S,Xsu}$	0.05	0.34	$K_{i,Snh3,Xpro}$	0.20	1.79	$f_{bu,su}$	2.72	20.48	$f_{bu,su}$	2.93	24.05	$f_{ac,su}$	0.81	15.33	$X_{ac,Batch7}$	1.89	11.52	$X_{ac,Batch7}$	2.73	13.98
$K_{S,Xaa}$	0.15	1.12	$K_{i,Snh3,Xac}$	0.16	1.55	$f_{ac,su}$	0.41	10.59	$f_{ac,su}$	0.48	12.46	$f_{h2,su}$	7.05	17.03	$X_{h2,Batch7}$	0.00	0.00	-	-	-
$K_{S,Xfa}$	0.15	3.83	$K_{i,Snh3,Xh2}$	0.24	1.70	$f_{h2,su}$	6.02	13.39	$f_{h2,su}$	5.83	13.35	$K_{i,Sh2,Xc4}$	0.03	0.40	-	-	-	-	-	-
$K_{S,Xc5}$	0.07	0.63	$f_{bu,su}$	3.56	30.53	$K_{i,Sh2,Xc4}$	0.33	4.00	$K_{i,Sh2,Xc4}$	0.16	4.36	$X_{ac,Batch7}$	1.63	7.72	-	-	-	-	-	-
$K_{S,Xc4}$	0.00	0.00	$f_{ac,su}$	0.67	17.63	$K_{i,Sh2,Xpro}$	0.17	1.55	$K_{i,Sh2,Xpro}$	0.13	2.88	$X_{h2,Batch2}$	0.07	1.00	-	-	-	-	-	-
$K_{S,Xpro}$	0.00	0.00	$f_{h2,su}$	7.20	16.29	$X_{su,Batch6}$	0.06	0.69	$X_{c4,Batch2}$	0.06	0.28	$X_{h2,Batch6}$	0.00	0.00	-	-	-	-	-	-
$K_{S,Xac}$	0.13	1.13	$K_{i,Sh2,Xfa}$	0.00	0.00	$X_{aa,Batch6}$	0.02	0.38	$X_{c4,Batch6}$	0.06	0.33	$X_{h2,Batch7}$	0.40	3.15	-	-	-	-	-	-
$K_{S,Xh2}$	0.79	4.53	$K_{i,Sh2,Xc5}$	0.03	0.88	$X_{aa,Batch7}$	0.00	0.00	$X_{c4,Batch7}$	0.00	0.00	-	-	-	-	-	-	-	-	-
$pH_{LL,ac}$	6.73	16.94	$K_{i,Sh2,Xc4}$	0.22	2.74	$X_{fa,Batch1}$	0.03	0.10	$X_{pro,Batch1}$	0.05	0.44	-	-	-	-	-	-	-	-	-
$K_{i,Snh3,Xc5}$	0.02	0.29	$K_{i,Sh2,Xpro}$	0.25	2.26	$X_{fa,Batch2}$	0.00	0.00	$X_{pro,Batch2}$	0.00	0.00	-	-	-	-	-	-	-	-	-
$K_{i,Snh3,Xc4}$	0.16	2.64	k_La	0.07	0.39	$X_{fa,Batch6}$	0.00	0.00	$X_{pro,Batch6}$	0.05	0.64	-	-	-	-	-	-	-	-	-
$K_{i,Snh3,Xpro}$	0.33	4.71	$X_{su,Batch1}$	0.05	0.47	$X_{fa,Batch7}$	0.07	0.69	$X_{pro,Batch7}$	0.20	1.12	-	-	-	-	-	-	-	-	-
$K_{i,Snh3,Xac}$	0.99	6.99	$X_{su,Batch2}$	0.03	0.28	$X_{c5,Batch1}$	0.00	0.01	$X_{ac,Batch1}$	0.15	1.09	-	-	-	-	-	-	-	-	-
$K_{i,Snh3,Xh2}$	0.23	3.55	$X_{su,Batch6}$	0.22	3.38	$X_{c5,Batch2}$	0.16	0.72	$X_{ac,Batch2}$	0.14	0.38	-	-	-	-	-	-	-	-	-
$f_{bu,su}$	1.97	24.39	$X_{su,Batch7}$	0.04	0.29	$X_{c5,Batch6}$	0.03	0.14	$X_{ac,Batch6}$	0.16	1.89	-	-	-	-	-	-	-	-	-
$f_{ac,su}$	0.56	13.69	$X_{aa,Batch1}$	0.05	0.60	$X_{c5,Batch7}$	0.07	0.26	$X_{ac,Batch7}$	1.99	7.48	-	-	-	-	-	-	-	-	-
$f_{h2,su}$	4.53	12.54	$X_{aa,Batch2}$	0.00	0.00	$X_{c4,Batch1}$	0.06	0.76	$X_{h2,Batch1}$	0.18	0.74	-	-	-	-	-	-	-	-	-
Σ IE (%) =	40.67	-	-	45.46	-	-	50.46	-	-	46.38	-	-	46.94	-	-	45.57	-	-	44.21	-
Total (%) =	72.37	-	-	75.17	-	-	78.67	-	-	74.74	-	-	72.81	-	-	70.49	-	-	68.79	-

Table 6. Calibration of potentially-identifiable input parameters (θ'): Prior and posterior distributions

Parameter	Units	Initial Value	Initial Evaluation Range		Posterior Parameter Distribution						
			Minimum	Maximum	Mean	Median	Mode	5% Percentile	95% Percentile	Skewness	Kurtosis
$K_{h,pr}$	d^{-1}	0.050	0.005	0.095	0.048	0.048	0.044	0.040	0.057	0.217	2.83
$K_{h,ch,slow}$	d^{-1}	0.0120	0.0012	0.0228	0.0109	0.0108	0.0102	0.0084	0.0137	0.171	2.74
$k_{m,fa}$	d^{-1}	10.0	1.0	19.0	7.3	6.8	6.6	4.6	12.0	1.663	6.93
$k_{m,c5}$	d^{-1}	8.0	0.8	15.2	10.4	10.3	8.6	7.2	13.4	0.084	2.75
$k_{m,c4}$	d^{-1}	13.0	1.3	24.7	19.6	19.5	20.2	15.8	23.6	0.001	2.52
$k_{m,pro}$	d^{-1}	10.0	1.0	19.0	12.2	12.2	13.0	7.1	16.7	-0.148	2.66
$k_{m,ac}$	d^{-1}	16.0	1.6	30.4	24.2	24.5	23.2	18.7	29.4	-0.242	2.32
$k_{m,h2}$	d^{-1}	20.0	2.0	38.0	26.0	25.5	25.1	17.0	36.1	0.077	2.19
k_d	d^{-1}	0.040	0.004	0.076	0.040	0.040	0.045	0.020	0.059	-0.155	2.83
pH_{LLac}		5.8	5.0	6.9	5.4	5.4	5.2	5.0	5.9	0.589	2.73
$X_{ac,Batch7}$	kg COD m^{-3}	-2.523	-3.784	-1.261	-2.648	-2.713	-2.853	-3.574	-1.543	0.303	2.39
$f_{bu,su}$	kg COD kg COD^{-1}	0.50	0.05	0.95	0.54	0.54	0.49	0.38	0.72	0.161	2.67
$f_{ac,su}$	kg COD kg COD^{-1}	0.29	0.03	0.55	0.28	0.29	0.23	0.12	0.43	-0.180	2.73
$f_{h2,su}$	kg COD kg COD^{-1}	0.10	0.01	0.19	0.09	0.09	0.09	0.02	0.17	0.060	2.31

EXPERIMENTAL DATA

HS-AD batch experiments fed with OFMSW

TS ϵ [10-30] %

HYPOTHESIS

Reversible NH_3 inhibition in all VFA and H_2 degraders

$$I_{nh3} = \frac{K_{i,Snh3}}{K_{i,Snh3} + S_{nh3,App}}$$

MODEL DEVELOPMENT

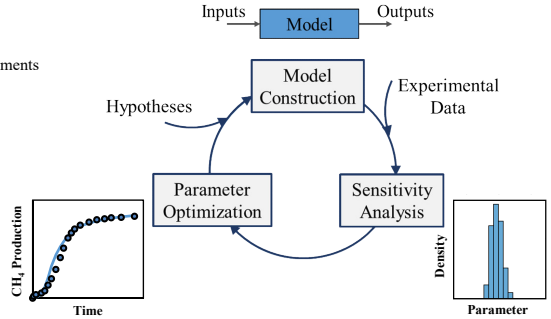

CONCLUSIONS

- Ionic Strength ≥ 0.9 M;
- NH_3 ≥ 2.3 g N/L;
- Highly correlated parameters;
- Extensive experimental data needed to avoid non-identifiability;
- The reversible function poorly represents NH_3 inhibition.